Band-structure calculation of dispersion and anisotropy in $\overleftrightarrow{\chi}^{(3)}$ for third-harmonic generation in Si, Ge, and GaAs

D. J. Moss,* E. Ghahramani, J. E. Sipe, and H. M. van Driel
Department of Physics, University of Toronto, Toronto, Ontario, Canada M5S 1A7
(Received 10 July 1989)

We perform a full band-structure calculation of the dispersion, anisotropy, and magnitude of the nonlinear response $\overleftrightarrow{\chi}^{(3)}$ for optical third-harmonic generation in Si, Ge, and GaAs, using both an empirical tight-binding (ETB) and a semi–*ab initio* band-structure technique. The calculation is performed with use of standard perturbation theory within the random-phase approximation and neglect of local-field corrections, with the minimal-coupling interaction Hamiltonian. The sign of $\overleftrightarrow{\chi}^{(3)}(0)$ is positive, independent of the tight-binding approximation, and in agreement with experimental results from the literature. We find that intraband contributions to $\overleftrightarrow{\chi}^{(3)}$ are small, in contrast with earlier results obtained by using the dipole interaction Hamiltonian. While both expressions for $\overleftrightarrow{\chi}^{(3)}$ yield a positive $\overleftrightarrow{\chi}^{(3)}(0)$, the minimal-coupling expression is dominated by the interband response, whereas the dipole expression is dominated by the intraband response. The resulting anisotropy in $\overleftrightarrow{\chi}^{(3)}$ obtained from the ETB bands for all materials agrees with the experiment better than other calculations to date at frequencies far below the optical band gap. For silicon, the anisotropy calculated from the ETB band structure also agrees well with recent measurements on the dispersion of the anisotropy at frequencies comparable to the optical band gap. The values of $|\overleftrightarrow{\chi}^{(3)}(0)|$ obtained from the ETB bands overestimate the experimental values by factors of 2 (for Si and GaAs) to 5 (for Ge), while the results obtained from the semi–*ab initio* bands underestimate the experimental values by a factor of approximately 2 (for Si) and 7 (for Ge and GaAs). While the (ETB) results for Si and GaAs are approximately within experimental error, the difference between the results from the two band-structure calculations reflects the high sensitivity of $\overleftrightarrow{\chi}^{(3)}$ to the details of the energy bands and wave functions.

I. INTRODUCTION

Although the field of nonlinear optics is over a quarter-century old, the number of full band-structure calculations of the nonlinear-optical constants for solids is very small.[1–4] The primary difficulty is the complexity of the nonlinear response function itself, combined with the requirement of knowing both the electronic energy bands and wave functions throughout the Brillouin zone. The earliest approaches to calculating both $\overleftrightarrow{\chi}^{(2)}$ and $\overleftrightarrow{\chi}^{(3)}$ for solids used a bonding–molecular-orbital technique[5–7] that was unable to predict the dispersion of the nonlinear coefficients. Another approach is to model the bands only around a few principal critical points in the band structure, and this has been used to calculate $\overleftrightarrow{\chi}^{(3)}$ associated with the Franz-Keldysh effect at zero frequency.[8,9] Although the dispersion in $\overleftrightarrow{\chi}^{(2)}$ for semiconductors has been calculated[1,2] the dispersion in $\overleftrightarrow{\chi}^{(3)}$ has not. The third-order susceptibility of cubic semiconductors is perhaps more interesting than $\overleftrightarrow{\chi}^{(2)}$ since there are two nonzero independent elements of $\overleftrightarrow{\chi}^{(3)}$ [for third-harmonic generation (THG)] given by $\overleftrightarrow{\chi}^{(3)}_{1111} \equiv A$ and $\overleftrightarrow{\chi}^{(3)}_{1212} \equiv B/3$, and from which we can define the anisotropy parameter[7,10] $\sigma \equiv (B-A)/A$ that vanishes for an isotropic system. Since the anisotropy is a relative quantity, it is easier to determine experimentally than the absolute magnitude of $\overleftrightarrow{\chi}^{(3)}$, and is interesting because it is not determined by symmetry, but rather is sensitive to the microscopic electronic properties of the solid. One of the primary failings of most calculations of $\overleftrightarrow{\chi}^{(3)}$ to date has been the inability to predict anisotropies at zero frequency [$\sigma(0)$] which are in reasonable agreement with experiment. The best results for $\sigma(0)$ to date were obtained by including local-field corrections. It is of interest, therefore, to see if a full band-structure calculation (without local-field corrections) is capable of producing reasonable values for the anisotropy, at frequencies both well below and comparable to the optical band gap. The dispersion in the anisotropy is of particular interest in light of recent experiments[11,12] measuring dispersion in the anisotropy of $\overleftrightarrow{\chi}^{(3)}$ at frequencies near the band gap in silicon and germanium.

Recently, we have been successful in using a simple empirical tight-binding (ETB) band-structure technique to calculate dispersion in the linear-[13] and second-order nonlinear-optical[1] constants for semiconductors. In this paper we adopt the same approach to calculate both the dispersion and zero-frequency limit of the absolute magnitude and anisotropy of the nonlinear response $\overleftrightarrow{\chi}^{(3)}$ responsible for optical THG in Si, Ge, and GaAs. We also use a semi–*ab initio* band structure[14] to calculate $\overleftrightarrow{\chi}^{(3)}$ and compare the results both with the ETB approach and with experiment.

In order to identify different contributions to $\overleftrightarrow{\chi}^{(3)}$ from many-particle excited states of the system, we present in some detail the derivation of the theoretical expression

for $\overleftrightarrow{\chi}^{(3)}$ in the Appendix. The calculation is carried out using standard perturbation theory within the Pines-Bohm random-phase approximation (RPA), and neglecting local-field corrections. We use the minimal coupling (MC), or "$\mathbf{p}\cdot\mathbf{A}$," interaction Hamiltonian, rather than the dipole Hamiltonian. Although $\overleftrightarrow{\chi}^{(3)}$ satisfies gauge invariance,[12] one must be particularly careful when using the dipole Hamiltonian in solids, where the interaction matrix elements $\langle \mathbf{r} \rangle$ become singular.[15,16] While this has been correctly addressed for $\overleftrightarrow{\chi}^{(2)}$ (Ref. 15) and $\overleftrightarrow{\chi}^{(3)}$ (Ref. 9), it has led to incorrect expressions for $\overleftrightarrow{\chi}^{(3)}(0)$ in the literature.[4] Use of the MC interaction Hamiltonian avoids this difficulty since the momentum matrix elements are well defined. We identify contributions to $\overleftrightarrow{\chi}^{(3)}$ that contain diagonal momentum matrix elements ($\mathbf{p}_{ii}\sim\nabla_{\mathbf{k}}$) as "intraband" contributions which vanish in the limit of localized electron states. One might expect these contributions to correspond with the intraband terms discussed with respect to the Franz-Keldysh effect at zero frequency,[8,9] but the relative contribution of the intraband terms to $\overleftrightarrow{\chi}^{(3)}(0)$ differs for the minimal-coupling and dipole forms of $\overleftrightarrow{\chi}^{(3)}(0)$. While both methods yield a positive value for $\overleftrightarrow{\chi}^{(3)}(0)$, the dipole expression is dominated by the intraband component, whereas the minimal-coupling Hamiltonian is dominated by the interband component. This phenomenon has been previously noted for $\overleftrightarrow{\chi}^{(2)}$.[15] We find that the minimal-coupling expression for $\overleftrightarrow{\chi}^{(3)}(0)$ should, in general, be positive. This is gratifying, since all measured values for $\overleftrightarrow{\chi}^{(3)}(0)$ in cubic-symmetry group-IV materials and II-IV compounds (Ref. 17) are positive. An argument based on a simple two-level dipole expression[4] for $\overleftrightarrow{\chi}^{(3)}$ which predicts a negative $\overleftrightarrow{\chi}^{(3)}(0)$ is incorrect, because of the improper treatment of the Bloch-state dipole matrix elements, together with the physical limitations of a two-level system. In addition to the intraband contributions, we identify virtual-electron, virtual-hole, and three-state contributions. While the first two contributions have analogies in the expression for $\overleftrightarrow{\chi}^{(2)}$, the three-state contribution is unique to $\overleftrightarrow{\chi}^{(3)}$ (and higher-order nonlinearities) and exists because of the four virtual transitions in $\overleftrightarrow{\chi}^{(3)}$.

Our results obtained using the ETB band structures for all materials yield anisotropies that are in good agreement with experiment, not just at frequencies well below the band gap, but, for silicon, in regions where dispersion is important. Although the anisotropies (at low frequency) calculated from the semi-*ab initio* bands were typically a factor of 2–3 larger than experimental values, including local-field corrections would probably not improve our results since local-field corrections were seen to increase the anisotropy.[9] The results from the ETB calculation for the zero-frequency limit of the magnitude of $\overleftrightarrow{\chi}^{(3)}$ overestimate the experimental values by factors of 2 (for Si and GaAs) to 5 (for Ge), while the results from the semi-*ab initio* tight-binding bands underestimate the experimental values by factors of approximately 2 (for Si) and 7 (for Ge and GaAs). This agreement is relatively good, considering the experimental uncertainty of about a factor of 2. The poor result for Ge from the ETB bands arises because the effective mass of the lowest conduction band at the Brillouin-zone center is overestimated. The different results obtained from the two band structures for the magnitude and anisotropy of $\overleftrightarrow{\chi}^{(3)}$ reflect the sensitivity of $\overleftrightarrow{\chi}^{(3)}$ to the electronic band structure, and so it would seem unreasonable to expect good results for $\overleftrightarrow{\chi}^{(3)}(0)$ by using either an over simplified band structure, or, in particular, a bonding–molecular-orbital technique. Although results for $\overleftrightarrow{\chi}^{(3)}(0)$ exist in the literature[9] which are somewhat closer to experiment than ours, they were obtained by using a limited band-structure theory which modeled the bands only around a few critical points, and this method did not succeed as well in predicting the dispersion in $\overleftrightarrow{\chi}^{(2)}$ (Ref. 18) as did full band-structure calculations.[1,2] The dispersion of $|\overleftrightarrow{\chi}^{(3)}(\omega)|$, on the other hand, shows very similar behavior for the ETB and semi-*ab initio* tight-binding band structures. However, since experimental data on the dispersion in the magnitude of $\overleftrightarrow{\chi}^{(3)}$ for the materials considered in this paper are limited to two wavelengths,[17,19] and have a large degree of uncertainty, comparison between theory and experiment for the dispersion in $\overleftrightarrow{\chi}^{(3)}$ is inconclusive.

In the next section we derive expressions for the nondivergent real and imaginary parts of $\overleftrightarrow{\chi}^{(3)}$ from a band-structure point of view and consider the physical interpretation of various contributions to $\overleftrightarrow{\chi}^{(3)}$ in terms of the many-particle excited states of the system. We also consider the gauge invariance of $\overleftrightarrow{\chi}^{(3)}$ and discuss the results of bonding–molecular-orbital calculations for $\overleftrightarrow{\chi}^{(3)}$. In Sec. III we discuss the electronic energy band structures and momentum matrix elements. In Sec. IV we consider the integration of the response function over the Brillouin zone, and in Sec. V the results are presented and compared with experiment. Finally, in Sec. VI conclusions are given.

II. NONLINEAR RESPONSE

The nonlinear response function ($\overleftrightarrow{\chi}^{(3)}$) for THG is related to the bulk nonlinear polarization via

$$P^{a}_{\mathrm{NL}}(3\omega)=\chi^{(3)}_{abcd}(-3\omega;\omega,\omega,\omega)\mathcal{E}^{b}(\omega)\mathcal{E}^{c}(\omega)\mathcal{E}^{d}(\omega)\ , \tag{1}$$

where Latin subscripts and superscripts indicate Cartesian components, and the summation over indices is implied. From the Appendix, the expression for $\overleftrightarrow{\chi}^{(3)}$ describing optical THG within the random-phase approximation and neglect of local-field corrections is

$$\chi^{(3)}_{abcd}(-3\omega;\omega,\omega,\omega)=+\frac{1}{3}\left[\frac{e}{m\omega}\right]^{4}\sum_{i,j,k,l}\int_{\mathrm{BZ}}\frac{d\mathbf{k}}{4\pi^{3}}G^{(3)}_{ijkl}(p^{a}_{ij}p^{b}_{jk}p^{c}_{kl}p^{d}_{li})\ , \tag{2}$$

where

$$G^{(3)}_{ijkl}=\frac{1}{3E-E_{ji}}\left[\frac{1}{2E-E_{ki}}\left[\frac{f_{il}}{E-E_{li}}+\frac{f_{kl}}{E-E_{kl}}\right]+\frac{1}{2E-E_{jl}}\left[\frac{f_{kj}}{E-E_{jk}}+\frac{f_{kl}}{E-E_{kl}}\right]\right],$$

$E=\hbar\omega$, $E_{ji}=E_j-E_i$, $f_{ij}=f_i-f_j$, etc., where f_i is the Fermi occupation factor of the single-particle state i. The p^a_{ij}, etc. are Bloch-state momentum matrix elements, and appear because the minimal-coupling interaction Hamiltonian was used. In Eq. (2), the indices i,j,k,l run over all single-particle states, the only restrictions arising from the Fermi factors. If one explicitly writes out all of the different terms, separating states into valence- and conduction-band states, one finds that there are five physically distinct contributions to $\overleftrightarrow{\chi}^{(3)}$: a virtual-electron, three virtual-hole, and a three-state contribution(s). These contributions are depicted in Fig. 1. The virtual-electron term involves the successive (virtual) excitation of an electron to two conduction bands, and then back to the valence band. Similarly, there is a single–virtual-hole contribution [Fig. 1(b)] involving the virtual excitation of a conduction-band hole to two successive valence bands and then back to the conduction band. The other two virtual-hole terms [Figs. 1(c)i and 1(c)ii] involve the successive excitation of both an electron and a hole. The three-state contribution is depicted in Fig. 1(d) for a one-particle system. For a many-particle system the three-state contribution is more complicated and we have not found a corresponding physical picture for the general case. However, we expect[12] that, in general, the three-state contribution will include terms involving the successive excitation of two electrons (rather than an electron and hole, as in the last two virtual-hole processes), in addition to the one-particle-like contribution shown in Fig. 1(d).

The virtual-electron (VE) contribution to $\overleftrightarrow{\chi}^{(3)}$ is given by

$$\overleftrightarrow{\chi}^{(3)}_{\rm VE}=-\frac{1}{3}\left[\frac{e}{m\omega}\right]^4\sum_{i,j,k,l}\int_{\rm BZ}\frac{d\mathbf{k}}{4\pi^3}\left[\frac{\mathbf{p}^{vc}_{ij}\mathbf{p}^{cc}_{jk}\mathbf{p}^{cc}_{kl}\mathbf{p}^{cv}_{li}}{(E_{ji}-3E)(E_{ki}-2E)(E_{li}-E)}+\frac{\mathbf{p}^{cc}_{kl}\mathbf{p}^{cv}_{li}\mathbf{p}^{vc}_{ij}\mathbf{p}^{cc}_{jk}}{(E_{li}-E)(E_{ki}+2E)(E_{ji}+E)}\right.$$
$$\left.+\frac{\mathbf{p}^{cv}_{li}\mathbf{p}^{vc}_{ij}\mathbf{p}^{cc}_{jk}\mathbf{p}^{cc}_{kl}}{(E_{li}+3E)(E_{ki}+2E)(E_{ji}+E)}+\frac{\mathbf{p}^{cc}_{jk}\mathbf{p}^{cc}_{kl}\mathbf{p}^{cv}_{li}\mathbf{p}^{vc}_{ij}}{(E_{li}-E)(E_{ki}-2E)(E_{ji}+E)}\right], \tag{3}$$

where now all the energy differences are defined as $E_{ji}=E^{\rm CB}_j-E^{\rm VB}_i$, etc., and so i refers to a valence-band (VB) state and j,k,l refer to conduction-band (CB) states, as indicated by superscripts on the momentum matrix elements. This equation is valid for any crystal class. We consider the simplification of Eq. (3) for cubic-symmetry crystals later. The virtual-hole terms can be obtained from the virtual-electron term by the prescription outlined in Table I. [Note that the last two virtual-hole terms have an overall minus sign. This arises from the anticommutation relations (see the Appendix) and occurs because the transitions shown in Fig. 1(c) involve successive excitations of *different* electrons, and the total wave function of the system must be antisymmetric.]

The expression for the three-state contribution is

$$\overleftrightarrow{\chi}^{(3)}_{\text{three-state}}=+\frac{1}{3}\left[\frac{e}{m\omega}\right]^4\sum_{i,j,k,l}\int_{\rm BZ}\frac{d\mathbf{k}}{4\pi^3}\left[\frac{\mathbf{p}^{ve}_{ij}\mathbf{p}^{cv}_{jk}\mathbf{p}^{vc}_{kl}\mathbf{p}^{cv}_{li}}{(E_{ji}-3E)(E_{lk}+E)}\left[\frac{1}{E_{li}-E}+\frac{1}{E_{jk}-E}\right]\right.$$
$$\left.+\frac{\mathbf{p}^{cv}_{li}\mathbf{p}^{vc}_{ij}\mathbf{p}^{cv}_{jk}\mathbf{p}^{vc}_{kl}}{(E_{li}+3E)(E_{jk}-E)}\left[\frac{1}{E_{ji}+E}+\frac{1}{E_{lk}+E}\right]\right], \tag{4}$$

which is, again, valid for any crystal class.

We now consider the effects of symmetry on $\overleftrightarrow{\chi}^{(3)}$. For THG there is only a single frequency present, and so $\overleftrightarrow{\chi}^{(3)}$ will be symmetric in the last three indices. In addition, for cubic materials all of the (x,y,z) directions are equivalent, and so there are only two nonzero independent elements of $\overleftrightarrow{\chi}^{(3)}$,[10] namely $A\equiv\chi^{(3)}_{1111}$ and $B\equiv 3\chi^{(3)}_{1212}=3\chi^{(3)}_{1221}=3\chi^{(3)}_{1122}$, and we

TABLE I. Virtual-electron and -hole contributions to $\overleftrightarrow{\chi}^{(3)}$ [the virtual-hole contributions to $\overleftrightarrow{\chi}^{(3)}$ can be obtained from the virtual-electron contribution, given by Eq. (3) in the text, using the substitutions for the energies and matrix elements shown here, together with the overall sign factor given in the last column].

Process	Figure	Energies[a]	Matrix elements	Overall sign[b]
Virtual-electron	1(a)	E_{ji},E_{ki},E_{li}	$\mathbf{p}^{vc}_{ij}\mathbf{p}^{cc}_{jk}\mathbf{p}^{cc}_{kl}\mathbf{p}^{cv}_{li}$	+
Virtual-hole	1(b)	E_{ji},E_{jl},E_{jk}	$\mathbf{p}^{vc}_{ij}\mathbf{p}^{vv}_{li}\mathbf{p}^{vv}_{kl}\mathbf{p}^{cv}_{jk}$	+
	1(c)i	E_{ji},E_{ki},E_{kl}	$\mathbf{p}^{vc}_{ij}\mathbf{p}^{cc}_{jk}\mathbf{p}^{vv}_{li}\mathbf{p}^{cv}_{kl}$	−
	(c)ii	E_{ji},E_{jl},E_{kl}	$\mathbf{p}^{vc}_{ij}\mathbf{p}^{vv}_{li}\mathbf{p}^{cc}_{jk}\mathbf{p}^{cv}_{kl}$	−

[a]Energies are defined as $E_{ij}=E^{\rm CB}_i-E^{\rm VB}_j$.

[b]The overall sign of the last two virtual-hole processes is negative. This arises from the electron anticommutation relations as discussed in the text.

can define a complex anisotropy[10] $\sigma \equiv (B-A)/A$ that vanishes for isotropic media. We consider various physical limits for the anisotropy later. Finally, time-reversal symmetry leads to

$$\{\mathbf{p}_{ij}\mathbf{p}_{jk}\mathbf{p}_{kl}\mathbf{p}_{li}\}_{\mathbf{k}}+\{\ \}_{-\mathbf{k}}=\{\ \}_{\mathbf{k}}+\{\ \}_{\mathbf{k}}^{*}\sim \mathrm{Re}\{\ \}_{\mathbf{k}}\ , \tag{5}$$

so only the *real* part of the matrix-element product survives.

An important consideration is the apparent divergence of Eq. (2) as $\omega\rightarrow 0$. For an intrinsic semiconductor at $T=0$ K, we expect $\overleftrightarrow{\chi}^{(3)}(0)$ to be finite. When the divergent pieces of Eq. (2) are identified, the term $\sim\omega^{-4}$ is[5]

$$\chi^{(3)}_{1111}\sim\frac{1}{\omega^4}\sum_{i,j}\int_{\mathrm{BZ}} f_0(E_{ji})\frac{\partial^4 E_{ji}}{\partial k_x^4}d\mathbf{k}\ , \tag{6}$$

where $f_0(E_{ji})$ is the Fermi occupation factor corresponding to the energy E_{ji}. This term has been discussed elsewhere[5] and, for an intrinsic semiconductor at $T=0$ K, it vanishes identically. For $T\neq 0$ K this term will dominate the response at sufficiently low frequencies or sufficiently high carrier concentrations. We assume $T=0$ K, and so ignore the contribution of this term. In addition, there is a contribution to Eq. (2) which varies as $\sim\omega^{-2}$. However, this term is substantially more complicated than Eq. (6) and, while we have not found a way to prove that this term vanishes, we expect that on physical grounds the terms which diverge as $\omega\rightarrow 0$ *must* vanish identically at $T\rightarrow 0$ K, and so we only consider the terms which are explicitly nondivergent as $\omega\rightarrow 0$. These terms can be separated out using partial fractions, and the real and imaginary parts of $\overleftrightarrow{\chi}^{(3)}$ can be obtained by letting $E=\hbar\omega+i\eta$ and taking the limit as $\eta\rightarrow 0$, in the same manner as for $\overleftrightarrow{\chi}^{(2)}$ and the linear response function. When all of this is done, the contribution of the virtual-electron process to the imaginary part of $\overleftrightarrow{\chi}^{(3)}$ becomes

$$\begin{aligned}\overleftrightarrow{\chi}''^{(3)}_{\mathrm{VE}}(\omega)=-\frac{\pi}{3}\left[\frac{e\hbar}{m}\right]^4\int_{\mathrm{BZ}}\frac{d\mathbf{k}}{4\pi^3}\sum_{i,j,k,l}\mathrm{Re}\{\mathbf{p}_{ij}^{vc}\mathbf{p}_{jk}^{cc}\mathbf{p}_{kl}^{cc}\mathbf{p}_{li}^{cv}\}\\ \times\left[\frac{3^6}{E_{ji}^4(3E_{ki}-2E_{ji})(3E_{li}-E_{ji})}\delta(E_{ji}-3E)\right.\\ +\frac{2^7(2E_{ji}-E_{ki})}{E_{ki}^4(2E_{li}-E_{ki})(2E_{ji}-3E_{ki})(2E_{ji}+E_{ki})}\delta(E_{ki}-2E)\\ \left.+\frac{1}{E_{li}^4(E_{ki}-2E_{li})}\left[\frac{1}{E_{ji}-3E_{li}}+\frac{2E_{ki}}{(E_{li}+E_{ji})(E_{ki}+2E_{li})}\right]\delta(E_{li}-E)\right]\ ,\end{aligned} \tag{7}$$

where the terms in large square brackets need not reflect the symmetry with respect to $j\leftrightarrow l$ since the indices are summed over. Terms in Eq. (7) where $j=k$ or $k=l$ contribute to the intraband response. It is straightforward to show that the contributions of multiple resonances (where, e.g., $E_{li}=3E_{ji}$) are, in fact, well behaved. The contribution of the virtual-hole processes can be obtained from Eq. (7) in the same manner as they were from Eq. (3), according to Table I. The contribution of the three-state term to the imaginary part of $\overleftrightarrow{\chi}^{(3)}$ is

$$\begin{aligned}\overleftrightarrow{\chi}''^{(3)}_{\text{three-state}}(\omega)=+\frac{\pi}{3}\left[\frac{e\hbar}{m}\right]^4\sum_{i,j,k,l}\int_{\mathrm{BZ}}\frac{d\mathbf{k}}{4\pi^3}\mathrm{Re}\{\mathbf{p}_{ij}^{vc}\mathbf{p}_{jk}^{cv}\mathbf{p}_{kl}^{vc}\mathbf{p}_{li}^{cv}\}\\ \times\left[\frac{3^6\delta(E_{ji}-3E)}{E_{ji}^4(3E_{jk}-E_{ji})(3E_{li}-E_{ji})}\right.\\ \left.+\frac{\delta(E_{li}-E)}{E_{li}^4(E_{jk}+3E_{li})}\left[\frac{E_{lk}+E_{jk}}{(E_{lk}-3E_{li})(E_{ji}+E_{li})}+\frac{E_{ji}+E_{jk}}{(E_{ji}-3E_{li})(E_{lk}+E_{li})}\right]\right]\ .\end{aligned} \tag{8}$$

As in the case of $\overleftrightarrow{\chi}^{(2)}$,[1] only the imaginary part of $\overleftrightarrow{\chi}^{(3)}$ need be evaluated explicitly from the band structure, which greatly simplifies the calculation.

We now briefly consider the dispersion in $\overleftrightarrow{\chi}^{(3)}(\omega)$ that one would expect from a given band structure. Since $\overleftrightarrow{\chi}^{(3)}$ is substantially more complicated than $\overleftrightarrow{\chi}^{(2)}$, relating features in the band structure to $\overleftrightarrow{\chi}^{(3)}(\omega)$ is more difficult. The imaginary part of $\overleftrightarrow{\chi}^{(3)}$ contains terms which are resonant with ω [$\sim\delta(E_{ji}-E)$], 2ω [$\sim\delta(E_{ki}-2E)$], and 3ω [$\sim\delta(E_{ji}-3E)$] and, since $\overleftrightarrow{\chi}^{(3)}$ is more complex than $\overleftrightarrow{\chi}^{(2)}$, the relatively uncommon[1,2] occurrence of double resonances in $\overleftrightarrow{\chi}^{(2)}$ will probably be more common in $\overleftrightarrow{\chi}^{(3)}$, with the additional (although unlikely) possibility of triple resonances. Due to its strong ($\sim E^{-7}$) energy dependence, $\overleftrightarrow{\chi}^{(3)}$ will be dominated by the 3ω resonance with the E_0 critical point[20] in materials where the lowest conduction band at the Brillouin-zone center is nondegenerate (such as Ge and GaAs). This enhancement will be larger in Ge than GaAs, since the direct band gap (E_0) lies much lower relative to the E_1 or E_2 optical peaks in Ge than it does in GaAs.

The anisotropy, however, is a relative quantity and so

the strong frequency dependence in the magnitude of both components of $\overleftrightarrow{\chi}^{(3)}$ is normalized out. As a result, the ω-resonant terms can contribute as much as, or even more than, the 2ω- or 3ω-resonant terms to the structure in $\sigma(\omega)$. But since σ depends in detail on the structure and symmetry of both the wave functions and energy bands throughout the Brillouin zone, it is difficult to predict the dispersion in the anisotropy in a straightforward manner.

We now consider the sign of $\overleftrightarrow{\chi}^{(3)}(0)$. For tetrahedral solids modeled with a minimal sp^3 basis set, the energy bands become twofold degenerate in the tight-binding limit. The expression for $\overleftrightarrow{\chi}^{(3)}(0)$ of a *localized* single-particle two-level system with states $|0\rangle$ and $|1\rangle$ and energy difference $E_g=E_1-E_0$ is given, using the dipole interaction Hamiltonian, by[12]

$$\overleftrightarrow{\chi}^{(3)}(0)=\frac{4}{E_g^3}|\boldsymbol{\mu}_{10}|^2[(\Delta\boldsymbol{\mu})^2-|\boldsymbol{\mu}_{10}|^2]\ , \tag{9}$$

with

$$\Delta\boldsymbol{\mu}=\boldsymbol{\mu}_{11}-\boldsymbol{\mu}_{00},\quad \boldsymbol{\mu}_{10}=\langle 1|\boldsymbol{\mu}|0\rangle\ ,$$

where $\boldsymbol{\mu}$ is the dipole moment operator. For a system with inversion symmetry $\Delta\boldsymbol{\mu}$ is zero, and so $\overleftrightarrow{\chi}^{(3)}(0)$ is negative. This equation has been used[4] to argue that $\overleftrightarrow{\chi}^{(3)}$ for a solid in the tight-binding limit is negative. In a solid, however, the matrix elements of $\boldsymbol{\mu}$ appearing in Eq. (9) are singular, and one must treat them in the same manner as in Refs. 15 and 16 before performing the integration over the Brillouin zone. The term in Eq. (9) proportional to $(\Delta\boldsymbol{\mu})^2$ is the analogue (for a localized system) of the intraband terms for a solid, and the results of Refs. 9 and 15 indicate that this term does not vanish in a solid, even with inversion symmetry. In any case, Eq. (9) as written is not well defined for a solid.

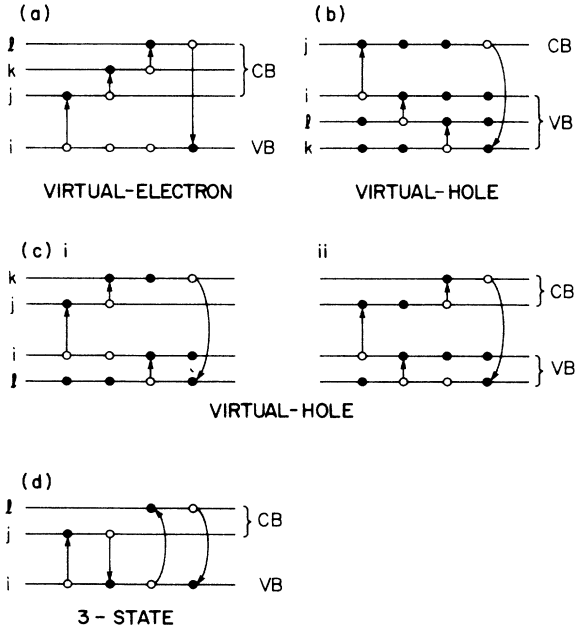

FIG. 1. Contributions to $\overleftrightarrow{\chi}^{(3)}$ from different single-particle processes. (a) Virtual electron, (b) and (c) virtual hole, and (d) three-state contributions.

The expression for $\overleftrightarrow{\chi}^{(3)}$ obtained using the MC interaction Hamiltonian is the same for either a localized two-level single-particle system or a solid (with a minimal sp^3 basis set) in the tight-binding limit, and is given by[12]

$$\overleftrightarrow{\chi}^{(3)}(0)=+\frac{1}{3}\left[\frac{e\hbar}{m}\right]^4|\mathbf{p}_{10}|^4\left[\frac{1}{E_g^7}\right]\times[(3^5+1)+3(3^3+1)+3^2(3+1)]\ . \tag{10}$$

This corresponds to the three-state term, and it is clear that it is always *positive*. Now for a solid, when the tight-binding condition is relaxed, one might expect $\overleftrightarrow{\chi}^{(3)}(0)$ to still be dominated by the (positive) three-state term, since most of the other terms contain conduction-band–conduction-band (c-c) matrix elements which vanish at the Brillouin-zone center for media with inversion symmetry. This, in fact, was found to be the case (see Sec. V). Therefore, from Ref. 9 we see that both the MC and dipole interaction Hamiltonians yield a positive value for $\overleftrightarrow{\chi}^{(3)}(0)$ in a solid; the difference is that the relative contribution of the intraband terms are not the same for the two cases. This feature, in fact, has already been noticed[15] in connection with $\overleftrightarrow{\chi}^{(2)}$, where the MC expression for $\overleftrightarrow{\chi}^{(2)}(0)$ actually contained *no* intraband contributions, while the dipole expression did. As in that case, the separation of interband and intraband terms is not gauge invariant.

We now consider what various models predict for the anisotropy of $\overleftrightarrow{\chi}^{(3)}$, and consider a molecular-orbital approach first. For a tetrahedrally coordinated system of four bonds, it is straightforward[12,21] to show that for one-dimensionally polarizable bonds, $\sigma=2$; for isotropic bonds, $\sigma=0$; and for ellipsoidally polarizable bonds, $0<\sigma<2$. One approach[5-7] is to treat the response of a tetrahedral molecule as a first approximation to a tetrahedrally bonded solid. In the simplest case, one considers only the valence s and p atomic orbitals, and forms bonding and antibonding orbitals pointing in the directions of the four nearest-neighbor atoms ($\hat{\mathbf{t}}_m$). If one then only considers transitions between orbitals pointing in the same direction,[5] one obtains

$$\langle b_m|\mathbf{p}|a_m\rangle\sim\hat{\mathbf{t}}_m,\quad \langle a_m|\mathbf{p}|a_m\rangle=\mathbf{0}\ , \tag{11}$$

so that both the minimal-coupling and multipole expressions for $\overleftrightarrow{\chi}^{(3)}$ yield an anisotropy equal to that for the system of one-dimensional bonds ($\sigma=2$).

Another common[5,6] approach to calculating $\overleftrightarrow{\chi}^{(3)}(0)$ for localized systems is to approximate all of the energy denominators in the expression for $\overleftrightarrow{\chi}^{(3)}(0)$ with a common energy gap, and then use closure to obtain[5,12]

$$\overleftrightarrow{\chi}^{(3)}_{\rm DP}(0)\simeq\frac{4}{E_g^3}(\langle\bar{\boldsymbol{\mu}}\bar{\boldsymbol{\mu}}\bar{\boldsymbol{\mu}}\bar{\boldsymbol{\mu}}\rangle-2\langle\bar{\boldsymbol{\mu}}\bar{\boldsymbol{\mu}}\rangle\langle\bar{\boldsymbol{\mu}}\bar{\boldsymbol{\mu}}\rangle)\ . \tag{12}$$

The first term in this expression is proportional to the sexadecapole of the ground-state charge distribution, and so for a tetrahedral system of bonding orbitals Eq. (12)

will give an anisotropy within the limits $0<\sigma<2$; the precise value cannot be determined without knowing the exact functional form of the orbitals. This result has provided the motivation for a calculation based on an expanded basis set,[7] and has yielded results closer to experiment than the result for one-dimensional bonds.

Both of these approaches neglect the translational symmetry of the solid, while the first approach suffers from the obvious drawback that, for a system of four degenerate ground states and four degenerate excited states, one should use degenerate perturbation theory. Clearly, the only appropriate way to calculate the anisotropy is to evaluate the full expression for $\overleftrightarrow{\chi}^{(3)}$ using the minimal-coupling Hamiltonian and a full electronic band structure. In the next section we briefly discuss the electronic band structures used in this calculation.

III. ELECTRONIC ENERGY BAND STRUCTURE

The ETB band structure we adopt in this paper was previously developed[13] to calculate the linear-optical properties for a wide range of semiconductors, and the second-order nonlinear-optical constant ($\overleftrightarrow{\chi}^{(2)}$) for zinc-blende–structure semiconductors.[1] We refer the reader to Ref. 13 for details of the formalism, and focus only on the features which differ for this calculation. In particular, while the results for the dispersion in $\epsilon(\omega)$ were good for all materials considered in this paper, the ETB bands for Ge and GaAs underestimated the effective mass of the lowest conduction band at the Brillouin-zone center. Since $\overleftrightarrow{\chi}^{(3)}$ is much more sensitive to the joint density of states (JDOS) than are the linear-optical properties, particularly around the band edge, we extend the earlier ETB calculation to include wave-function overlap. In doing this, we find that the conduction-band effective mass is considerably improved.

In order to calculate both the orbital-overlap integrals and the momentum matrix elements, we use the valence s and p wave functions obtained by Huang and Ching[14] in their semi–*ab initio* tight-binding band-structure calculation. The orbitals are of the form

$$S_{\mathrm{I,II}}(\mathbf{r})=\sum_i \Omega_{s_i} C^{S_i}_{\mathrm{I,II},i} e^{-\alpha_i r^2}\,,$$
$$P^x_{\mathrm{I,II}}(\mathbf{r})=r\sum_i \Omega_{p_i} C^{P}_{\mathrm{I,II},i} e^{-\alpha_i r^2}\,, \tag{13}$$

with

$$\Omega_{s_i}=\left[\frac{2\alpha_i}{\pi}\right]^{3/4},\quad \Omega_{p_i}=2\sqrt{\alpha_i}\left[\frac{2\alpha_i}{\pi}\right]^{3/4},$$

where I,II refer to the location [I refers to a cation (e.g., Ga), while II refers to an anion (e.g., As) of the orbital], the α_i are a set of Gaussian exponents, and the Ω_{s_i} and Ω_{p_i} are normalization constants; there are corresponding equations for $P^y(\mathbf{r})$ and $P^z(\mathbf{r})$. The use of Gaussian orbitals allows for the analytic evaluation of the momentum matrix elements and overlap integrals between the localized orbitals. The ETB bands were obtained by using the calculated overlap integrals as fixed parameters, and proceeding as before.[13] The reader is referred to Ref. 12 for the values of the orbital parameters from the semi–*ab initio* tight-binding bands, and for the new ETB parameters. The energy bands for all materials are shown in Fig. 2. As can be seen, the effective mass for the lowest conduction band at the Γ point in the ETB bands for both Ge and GaAs is significantly reduced by including wave-function overlap.

In addition, we use the full semi–*ab initio* tight-binding bands of Huang and Ching[14] to calculate $\overleftrightarrow{\chi}^{(3)}$ for all three materials. Details of the band-structure theory are given in Ref. 14 and references therein, and we simply show the resulting band structures in Fig. 2. Although the valence and conduction bands include the effect of core states, the explicit contribution of the core states to $\overleftrightarrow{\chi}^{(3)}$ was not included since the highest-lying core states in these materials lie more than 80 eV below the valence-band maximum.

The momentum matrix elements for the ETB bands take the form

$$\mathbf{p}^{vc}_{ij}(\mathbf{k})=\sum_{m,n} U^*_{im} W_{jn} \sum_{\Delta\mathbf{R}} \langle b^m(0)|\mathbf{p}|a^n(\Delta\mathbf{R})\rangle e^{i\mathbf{k}\cdot\Delta\mathbf{R}}\,, \tag{14}$$

where $|b^m(0)\rangle, |a^m(\Delta\mathbf{R})\rangle$ are bonding and antibonding orbitals, respectively, pointing in one of the four bond directions (m),[13] $\Delta\mathbf{R}$ is a fcc lattice site, U_{im}, W_{jn} are the eigenvectors which diagonalize the 4×4 valence- or conduction-band Hamiltonians, respectively, and there are corresponding equations for the c-c' and v-v' matrix elements. The bonding and antibonding orbitals can be written in terms of the sp^3 hybrids,[13] and the hybrids, in turn, are linear combinations of the s and p orbitals on a particular atomic site. In order to form bonding or antibonding orbitals, the hybrid overlap (S) and polarity parameters (α_p) are needed;[13] the overlap parameter was calculated directly from the wave functions and the po-

TABLE II. Material parameters.

	Si	Ge	GaAs
$\epsilon_1(0)$ (experimental)	12.0	16.0	10.9
$\epsilon_1(0)$ (theory—ETB bands)	12.3	19.7	9.1
$\epsilon_1(0)$ (theory—semi–*ab initio* bands)	7.6	11.3	6.9
Hybrid overlap[a]	0.696	0.672	0.654
Bond polarity[a] (α_p)	0	0	0.5
Lattice constants (Å)	5.431	5.658	5.654

[a]Following the definitions of Ref. 13.

larity parameter for GaAs was taken from Ref. 13. These parameters are shown in Table II. The momentum matrix elements could be calculated by including either all nearest-neighbor (NN) interactions in Eq. (14) to convergence (seventh-nearest neighbors), or by truncating the sum at any of the nearest-neighbor bonds as defined in Ref. 13. The momentum matrix elements for both the ETB bands and semi-*ab initio* tight-binding bands are shown in Table III. All matrix elements in Table III were calculated to convergence, but the results for the ETB bands where the sum in Eq. (14) was truncated at the "Y,Z" matrix elements[13] differed by less than 5%.

Since $\overleftrightarrow{\chi}^{(3)}$ depends on momentum matrix elements to the fourth power, it is of interest to have an independent means of estimating these matrix elements. From $\mathbf{k}\cdot\mathbf{p}$ perturbation theory,[22] one can relate the momentum matrix elements at particular $\mathbf{k}$ point to the energy-band effective mass. The relations at the Brillouin-zone center (Γ point) are summarized in Ref. 1, while for homopolar solids one must also focus on a $\mathbf{k}$ point other than the

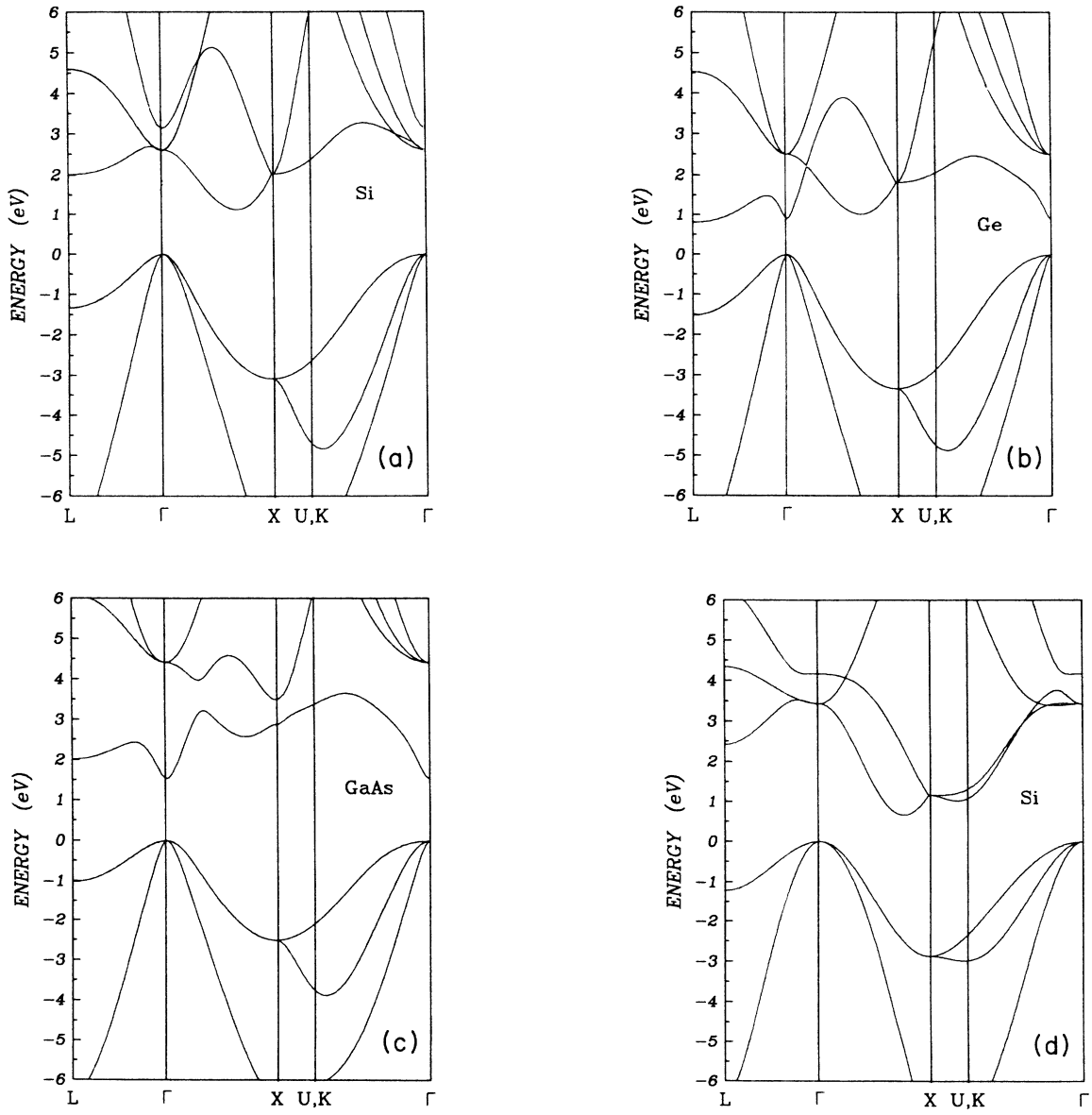

FIG. 2. Energy bands for semi-*ab initio* tight-binding bands for (a) Si, (b) Ge, and (c) GaAs, and ETB bands for (d) Si, (e) Ge, and (f) GaAs. For Ge and GaAs, the solid lines represent the bands used in our calculations and include wave-function overlap, while, for comparison, the dashed lines represent the bands of Ref. 13 that do not include wave-function overlap. The empirical band parameters are given in Ref. 12.

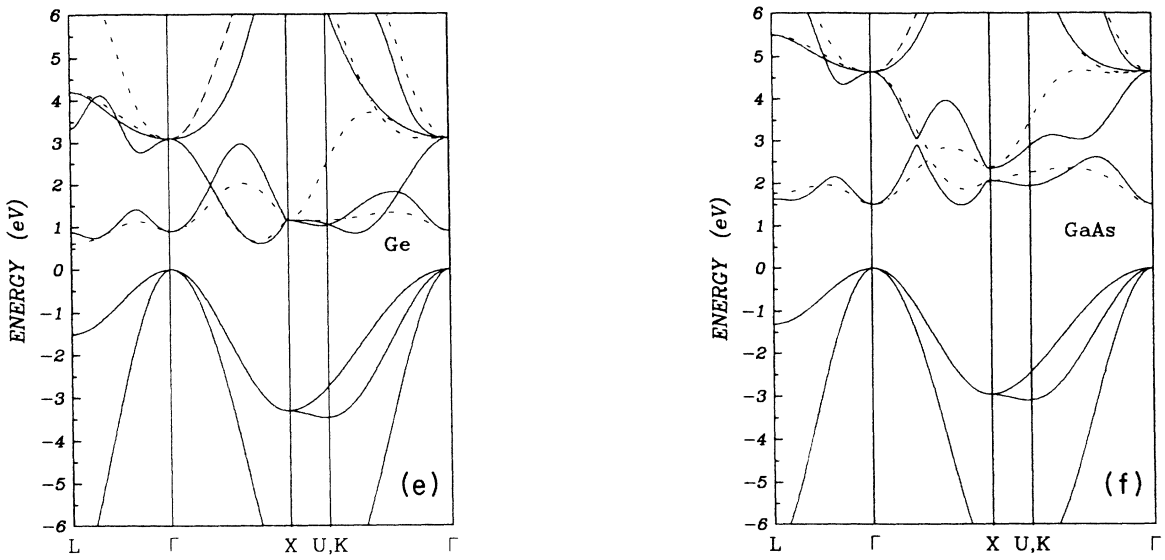

FIG. 2. (*Continued*).

Brillouin-zone center, since the c-c' matrix element is zero at this point. We therefore also focus on the conduction-band minimum ($\mathbf{k}_{\min}$) in silicon (along the [100] direction). If we number the energy bands in order of increasing energy at $\mathbf{k}_{\min}$, we see that for Si the CB3 and CB4 states are doubly degenerate, as are the VB3 and VB4 states, and will therefore only contribute to the transverse effective mass. In addition, the $\mathbf{p}_{13}^{vc}$, $\mathbf{p}_{21}^{vc}$, and $\mathbf{p}_{12}^{cc}$ matrix elements are zero by symmetry, and so the only matrix element which contributes to the longitudinal effective mass is $\mathbf{p}_{11}^{vc}$. Both effective masses are then given by

$$\left[\frac{m}{m_{\parallel}^{*}}\right]_{ij}=\delta_{ij}+\frac{1}{m}\left\{\left\{\frac{[\mathbf{p}_{31}^{vc}\mathbf{p}_{13}^{cv}+\mathbf{p}_{41}^{vc}\mathbf{p}_{14}^{cv}]_{ij}}{E_{\mathrm{CB1}}-E_{\mathrm{VB3}}}-\frac{[\mathbf{p}_{31}^{cc}\mathbf{p}_{13}^{cc}+\mathbf{p}_{41}^{cc}\mathbf{p}_{14}^{cc}]_{ij}}{E_{\mathrm{CB3}}-E_{\mathrm{CB1}}}\right\}+(i\leftrightarrow j)\right\} \tag{15}$$

TABLE III. Momentum matrix elements (shown here are the magnitude of the matrix elements in units of $\hbar/a_b$. All matrix elements are evaluated to convergence).

	ETB bands			Semi-*ab initio* bands		
	Si	Ge	GaAs	Si	Ge	GaAs
$\mathbf{k}=0$ [a]						
v_0-c'	0.21	0.27	0.26	0.11	0.16	0.10
v-c	0.30	0.39	0.38	0.58	0.61	0.55
v-c'	0.39	0.39	0.38	0.45	0.48	0.46
c-c'	0	0	0.03	0	0	0.19
$\mathbf{k}=\mathbf{k}_{\min}$ [b]						
$\lvert\langle \mathrm{VB1}\rvert\mathbf{p}\rvert\mathrm{CB1}\rangle\rvert$ [c]	0.42			0.13		
$\lvert\langle \mathrm{VB3}\rvert\mathbf{p}\rvert\mathrm{CB1}\rangle\rvert$ [d]	0.48			0.52		
$\lvert\langle \mathrm{CB1}\rvert\mathbf{p}\rvert\mathrm{CB3}\rangle\rvert$ [d]	0.21			0.047		

[a]Matrix elements at $\mathbf{k}=0$ are defined as follows: for v_0-c', $|\langle\Gamma_1^v|\mathbf{p}|\Gamma_{15}^c\rangle|$; for v-c, $|\langle\Gamma_{15}^v|\mathbf{p}|\Gamma_1^c\rangle|$; for v-c', $|\langle\Gamma_{15}^v|\mathbf{p}|\Gamma_{15}^c\rangle|$; and for c-c', $|\langle\Gamma_1^c|\mathbf{p}|\Gamma_{15}^c\rangle|$.

[b]$\mathbf{k}_{\min}$ is the position of the conduction-band minimum for silicon. For the ETB bands it is at (0.77,0,0) and for the semi-*ab initio* tight-binding bands it is at (0.68,0,0) (in units of $2\pi/a_0$). The matrix elements at $\mathbf{k}_{\min}$ are numbered in order of increasing band energy.

[c]For $\mathbf{k}_{\min}$ in the [100] direction, this matrix element is $\sim\hat{\mathbf{x}}$, and therefore only contributes to the longitudinal effective mass.

[d]For $\mathbf{k}_{\min}$ in the [100] direction, this matrix element is $\sim\hat{\mathbf{x}}$ or $\hat{\mathbf{z}}$, and therefore only contributes to the transverse effective mass. Also, $|\langle \mathrm{VB3}|\mathbf{p}|\mathrm{CB1}\rangle|=|\langle \mathrm{VB4}|\mathbf{p}|\mathrm{CB1}\rangle|$, and similarly for the c-c' elements.

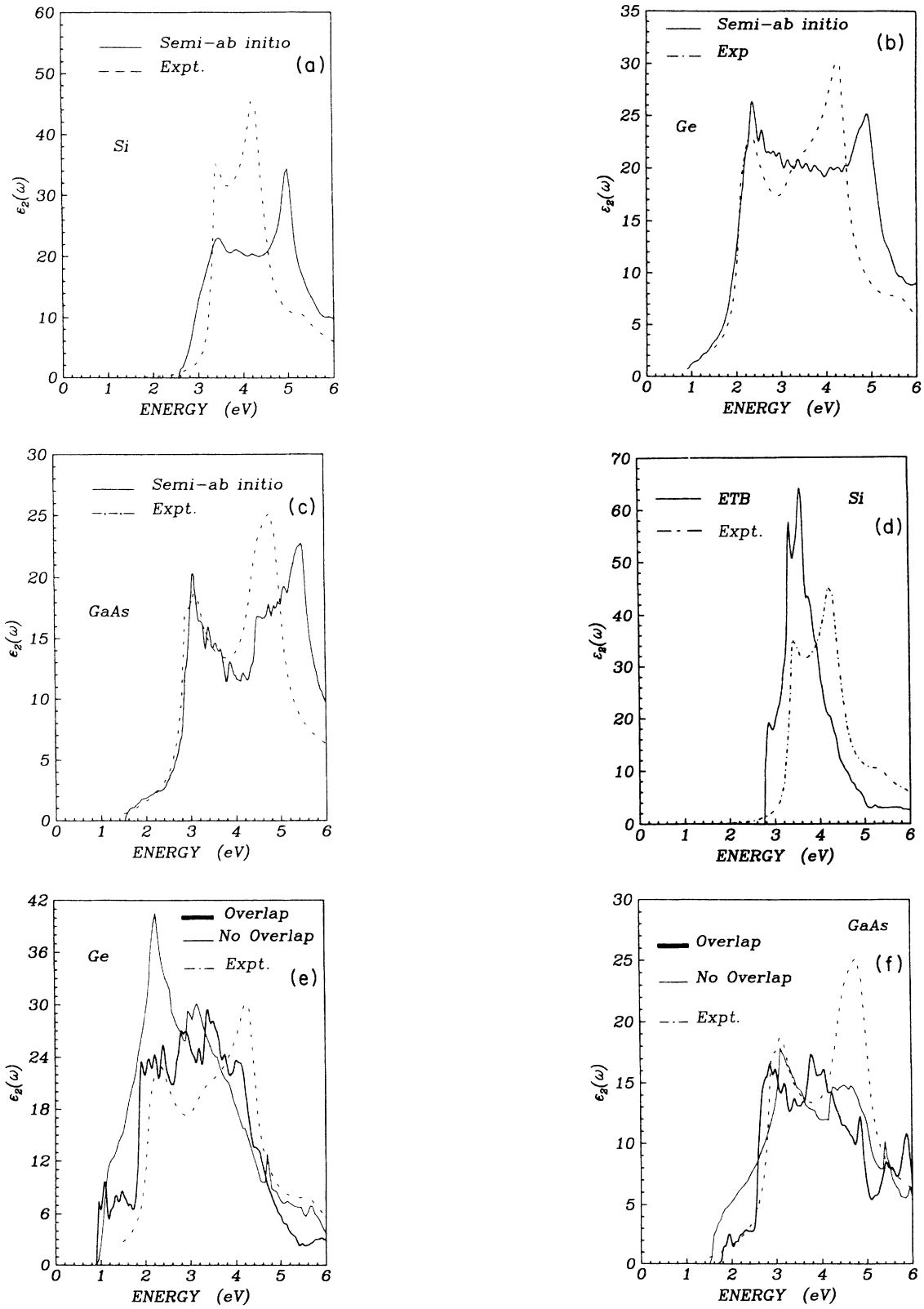

FIG. 3. Imaginary part of dielectric constant [$\epsilon_2(\omega)$] for the semi–*ab initio* tight-binding bands for (a) Si, (b) Ge and (c) GaAs, and for the ETB bands for (d) Si, (e) Ge, and (f) GaAs. For Ge and GaAs with the ETB bands, the heavy solid line is for the bands including wave-function overlap, while for comparison the light solid line is the result for the bands from Ref. 13 that do not include wave-function overlap. The dashed line is experiment [from D.E. Aspnes and (A. A. Studna, Phys. Rev. B **27**, 985 (1983)]. The results for the semi–*ab initio* tight-binding bands have been scaled to give the correct $\epsilon_1(0)$; the actual values of $\epsilon_1(0)$ obtained are given in Table II.

for the transverse effective mass, and

$$\left[\frac{m}{m_{\perp}^{*}}\right]_{ij}=\delta_{ij}+\frac{1}{m}\left\{\frac{[\mathbf{p}_{11}^{vc}\mathbf{p}_{11}^{cv}]_{ij}}{E_{\mathrm{CB1}}-E_{\mathrm{VB1}}}+(i\leftrightarrow j)\right\} \tag{16}$$

for the longitudinal effective mass. The theoretical and experimental conduction-band effective masses, at $\mathbf{k}_{\min}$ for Si and at Γ for all materials, are shown in Table IV. The agreement with experiment is quite good, particularly for the semi-*ab initio* tight-binding bands. The overestimation of the ETB effective masses for Ge and GaAs arises because the v-c matrix element (see Table III) are underestimated by $\sim 20-30\%$. The c-c' matrix elements at Γ (for GaAs) are significantly underestimated by the ETB bands, as previously noted,[1] but not so by the semi-*ab initio* tight-binding bands. This does not necessarily mean, however, that contributions to $\vec{\chi}^{(3)}$ for GaAs that include c-c' matrix elements (such as the virtual-electron contribution) will be significantly underestimated by the ETB bands, since $\vec{\chi}^{(3)}$ depends on the variation of the matrix elements throughout the Brillouin zone, not just at the Γ point. The slight disagreement between the conduction-band effective mass for GaAs shown in Table IV and that observed in Fig. 2 arises both because of the empirical nature of the bands and from the combined use of wave-function orbitals from a more fundamental theory.

Turning to the conduction-band minimum in Si, it is apparent that the ETB bands actually overestimate $\mathbf{p}_{11}^{vc}$ (see Tables III and IV), since $m_{\parallel}^{*}$ is underestimated. Although $m_{\perp}^{*}$ for Si is overestimated, we can only say that either $\mathbf{p}_{31}^{ve}$ is underestimated (as it is at Γ) or $\mathbf{p}_{13}^{cc}$ is overestimated. This does indicate, however, that the ETB bands probably do not underestimate the c-c' matrix elements as much at $\mathbf{k}_{\min}$ in Si as they do for zinc-blende semiconductors at the BZ center.[1] However, we point out that, in Si, $m_{\perp}^{*}$ is small because the interaction of the lowest conduction band with the upper two valence bands dominates, and so this method is relatively insensitive to the $\mathbf{p}_{13}^{cc}$ and $\mathbf{p}_{14}^{cc}$ matrix elements. Finally, we note the good agreement from the semi-*ab initio* tight-binding bands for the conduction-band effective mass in Si at $\vec{k}_{\min}$ suggests that the matrix elements in that case are probably accurate. Therefore, we see that the v-c momentum matrix elements calculated from the ETB band structure are underestimated by about 20%. The c-c' momentum matrix elements, on the other hand, are probably underestimated slightly more than this away from the Brillouin-zone center in Si, and substantially more than this for GaAs at the Brillouin-zone center. Finally, we see that the effective masses calculated with the semi-*ab initio* tight-binding bands for all materials agree quite well with experiment, both at and away from the Brillouin-zone center, and so the momentum matrix elements are probably more accurate than those obtained from the ETB bands.

The imaginary part of the dielectric constant $[\epsilon_2(\omega)]$ for all materials is shown in Fig. 3, while the results for the static dielectric constant $[\epsilon_1(0)]$ are given in Table II. While the ETB bands yielded and $\epsilon_1(0)$ for Si and GaAs nearly equal to experiment, and for Ge $\sim 20\%$ larger than experiment, there are compensating factors in these results. The ETB bands for Si and Ge (Ref. 13) shifted some of the oscillator strength to lower energy [thus increasing $\epsilon_1(0)$]. In Ge, this arose because the contribution of the E_0 critical point to $\epsilon_1(0)$ (even for the bands that include wave-function overlap) was overestimated. This effect is partially compensated for by the underestimation of the v-c momentum matrix elements discussed above. For GaAs the ETB bands with overlap did not significantly overestimate the conduction-band effective mass, and the underestimation of $\epsilon_1(0)$ is due solely, in this case, to the underestimation of the v-c matrix elements. The semi-*ab initio* tight-binding bands, on the other hand, consistently underestimate the experimental values of $\epsilon_1(0)$ by 30–40%. From Table III we see that this is primarily due to underestimating the JDOS at the critical points, rather than the matrix elements. We next consider the integration of the nonlinear-response function over the Brillouin zone.

IV. METHOD OF CALCULATION

A central difficulty in evaluating the nonlinear response of solids is integrating the response function over the Brillouin zone. If one is interested only in the zero-frequency limit, carrying out the integration is not so difficult since the response function often does not involve resonant energy denominators, and so one can use a simple sampling technique. However, frequency-

TABLE IV. Conduction-band effective masses (m^{*}/m) (the theoretical result is obtained using the $\mathbf{p}$ matrix elements from Table III).

	$\mathbf{k}=\mathbf{0}$[a]			Si: $\mathbf{k}=\mathbf{k}_{\min}$[b]	
	Si	Ge	GaAs	$m_{\parallel}^{*}/m$	$m_{\perp}^{*}/m$
Experiment[c]		0.04	0.07	0.92	0.19
Theory (ETB)	0.46	0.10	0.17	0.51	0.22
Theory (semi-*ab initio*)	0.15	0.04	0.09	0.93	0.21

[a]For the singly degenerate conduction band.
[b]$\mathbf{k}_{\min}$ is the conduction-band minimum.
[c]From Ref. 22.

dependent response functions usually involve resonant energy denominators. Our earlier calculation[1] for $\overleftrightarrow{\chi}^{(2)}$ used an extension of the linear analytic tetrahedra method (LATM) to nonlinear response functions[23] to perform the integration. However, $\overleftrightarrow{\chi}^{(3)}$ is much more complicated than $\overleftrightarrow{\chi}^{(2)}$, and we decided to use a sampling method. We evaluated the imaginary part of $\overleftrightarrow{\chi}^{(3)}$ first, and obtained the real part of $\overleftrightarrow{\chi}^{(3)}$ by using the Kramers-Kronig relations.[1] Typically, in using a sampling method, one can either linearize the energy bands over small integration cells, and then sample the linearized bands, or one can simply diagonalize the Hamiltonian at every sampling point. The latter method requires much more computer time than the former, but is more accurate. Since $\overleftrightarrow{\chi}^{(3)}$ is very sensitive to details of the energy bands, we decided to use the latter method. For the semi-*ab initio* tight-binding bands with ~60 000 sampling points in an irreducible $\frac{1}{48}$ sector of the first Brillouin zone, this required the use of ~2–3 hours of Cray Research, Inc. X-MP/22 supercomputer central-processing-unit (CPU) time per calculation. For all calculations, the energy resolution of the bin summation was 0.02 eV. Although the imaginary part of $\overleftrightarrow{\chi}^{(3)}$ [Eqs. (7) and (8)] does contain resonant energy denominators, it is straightforward to show that for cases where multiple resonances are satisfied (to within the resolution of the bin summation) the contribution of all of the resonant terms is well behaved. One *would* have a problem in evaluating the real part of $\overleftrightarrow{\chi}^{(3)}$, however, since this contains terms resonant in the excitation frequency rather than just the band energies. As a check on the calculation, $\overleftrightarrow{\chi}^{(3)}(0)$ was evaluated both by calculating the imaginary part of $\overleftrightarrow{\chi}^{(3)}$ and then using the Kramers-Kronig transformation, and also by integrating the expression for $\overleftrightarrow{\chi}^{(3)}(0)$ directly; the two results typically agreed to better than 5%.

The 48-fold symmetry of the Brillouin zone was taken into account by the following. If P_R is the operator for the Rth transformation of the cubic group, then the action of this on the following fourth-rank tensors gives

$$\begin{aligned}
&\sum_R P_R(\hat{x}\hat{x}\hat{x}\hat{x}) = 16\times(\hat{x}\hat{x}\hat{x}\hat{x}+\hat{y}\hat{y}\hat{y}\hat{y}+\hat{z}\hat{z}\hat{z}\hat{z}) ,\\
&\sum_R P_R(\hat{x}\hat{x}\hat{y}\hat{y}) = 8\times(\hat{x}\hat{x}\hat{y}\hat{y}+\hat{x}\hat{x}\hat{z}\hat{z}+\hat{y}\hat{y}\hat{x}\hat{x}\\
&\qquad\qquad +\hat{y}\hat{y}\hat{z}\hat{z}+\hat{z}\hat{z}\hat{x}\hat{x}+\hat{z}\hat{z}\hat{y}\hat{y}) ,
\end{aligned} \tag{17}$$

so that the contribution of the momentum matrix elements to the different components of $\overleftrightarrow{\chi}^{(3)}$ becomes

$$\begin{aligned}
A &\sim \sum_R P_R(p_x p_x p_x p_x) ,\\
B &\sim \sum_R P_R(p_x p_x p_y p_y) + \sum_R P_R(p_x p_y p_x p_y)\\
&\quad + \sum_R P_R(p_x p_y p_y p_x) .
\end{aligned} \tag{18}$$

Note that inversion has been included since, as mentioned above, the Brillouin zone always has inversion symmetry.

V. RESULTS

A. Zero-frequency limit of $\overleftrightarrow{\chi}^{(3)}$

The different contributions to $\overleftrightarrow{\chi}^{(3)}(0)$ for all three materials are shown in Table V. In all cases only the three-

TABLE V. Contributions to $\overleftrightarrow{\chi}^{(3)}(0)$. [$\overleftrightarrow{\chi}^{(3)}$ is in units of 1×10^{-11} esu. We use the definition of $\overleftrightarrow{\chi}^{(3)}$ from Ref. 5, which is a factor of 4 larger than the definition of Maker and Terhune (Ref. 25). The components of $\overleftrightarrow{\chi}^{(3)}(0)$ are $A\equiv\chi^{(3)}_{1111}$ and $B\equiv3\chi^{(3)}_{1212}$.]

	Si		Ge		GaAs	
	A	*B*	*A*	*B*	*A*	*B*
ETB bands						
Virtual-electron	−1.4	−0.9	−4.5	−2.8	−0.8	−0.6
Virtual-hole	−1.0	−1.8	−5.0	−6.7	−1.2	−1.8
Three-state	9.2	11.7	242.9	348.0	12.2	19.3
Total interband	6.8	9.0	233.4	338.5	10.2	16.9
Intraband	−2.0	−2.1	−27.4	−31.3	−2.2	−2.7
Total	4.8	6.9	206	307	8.0	14.2
Semi-*ab initio* bands						
Virtual-electron	−0.6	−1.0	−4.1	−7.0	−1.5	−1.7
Virtual-hole	−0.8	−1.6	−9.2	−17.1	−2.1	−2.5
Three-state	5.6	9.1	47.2	116.0	9.2	15.1
Total interband	4.2	6.5	33.9	92.0	5.6	10.9
Intraband	−3.5	−4.9	−27.0	−71.3	−4.9	−8.6
Total	0.8	1.6	6.9	20.7	0.7	2.3

TABLE VI. Results for $\chi^{(3)}_{1111}(0)$ (in units of 1×10^{-11} esu).

	Theory					Experiment
	ETB	Semi-*ab initio*	AJ[a]	BJ[b]	VA[c]	WB[d]
Si	4.8	0.8	0.26	−2.5	2.0	2.4±60%
Ge	206	7	0.67	−35	48	40±50%
GaAs	8.0	0.7		−5.0	4.8	3.9[e]

[a]From Ref. 4.
[b]From Ref. 5.
[c]From Ref. 8.
[d]From Ref. 17.
[e]From Ref. 26.

state term is positive, and dominates all of the other terms, including the intraband term. This is evidence that the expression for $\vec{\chi}^{(3)}(0)$ using the MC Hamiltonian is positive, both within and outside the tight-binding limit, since all terms except the three-state term vanish in this limit. From Table VI we see that the results for $\vec{\chi}^{(3)}(0)$ from the ETB bands range from approximately a factor of 2 (for Si and GaAs) to 5 (for Ge) larger than experiment. For Ge this difference is larger than the experimental uncertainty, and arises because of the overestimation of the conduction-band effective mass (at the Γ point) discussed earlier. By comparison, the conduction-band effective mass for GaAs was not overestimated, and so the result for $\vec{\chi}^{(3)}(0)$ is approximately within the experimental uncertainty. The values of $\vec{\chi}^{(3)}(0)$ obtained from the semi-*ab initio* tight-binding bands, in contrast, consistently underestimate values by about a factor of 2 for Si and 7 for Ge and GaAs. The situation is similar to that for the linear-optical properties, where we saw that the semi-*ab initio* tight-binding bands yielded values for $\epsilon(0)$ that were ~40% lower than those from the ETB bands. For $\vec{\chi}^{(3)}$, the difference between the two band structures is amplified further since $\vec{\chi}^{(3)}$ is much more sensitive to the details of the electronic band structure than $\epsilon(\omega)$ is. We note that, while our results for $\vec{\chi}^{(3)}(0)$ are not quite as good as the results of Ref. 8, their results were obtained by modeling the energy bands around the main critical points responsible for structure in the linear-optical spectrum. Our primary goal in this paper was to study the dispersion of $\vec{\chi}^{(3)}$, and in the case of $\vec{\chi}^{(2)}$ it was observed that the approach of modeling the energy bands around critical points did not succeed[18] in predicting the dispersion of $\vec{\chi}^{(2)}$ as well as full band-structure calculational methods did.[1,2] Our results for $\vec{\chi}^{(3)}(0)$ are much closer to experiment than the only other full band-structure calculation.[24]

B. Dispersion in $|\vec{\chi}^{(3)}|$

Figure 4 shows the dispersion of the two components of $|\vec{\chi}^{(3)}(\omega)|$ for Si, Ge, and GaAs for both band structures. For Si, $|\vec{\chi}^{(3)}(\omega)|$ obtained using both band structures is dominated by a large peak near $\hbar\omega=1.0$ eV arising from the 3ω resonance with the E_1 critical point. The smaller structure at $\hbar\omega\simeq1.5$ eV is due primarily to the 3ω resonance with the E_2 critical point—the 2ω resonances generally are quite small since the three-state term is dominant and it contains no 2ω-resonant contributions. The peak at ~1.0 eV is larger (relative to the peak at ~1.5 eV) in the ETB results compared to the semi-*ab initio* tight-binding results, because of the shift in oscillator strength discussed above. For Ge, $|\vec{\chi}^{(3)}(\omega)|$ obtained from both band structures is dominated by a large peak near $\hbar\omega\simeq0.3$ eV arising from the 3ω resonance with the direct band gap (E_0 optical peak). There is a smaller structure at $\hbar\omega\simeq0.7$ eV arising primarily from the 3ω resonance with the E_1 critical point. For GaAs, on the other hand, both band structures show con-

TABLE VII. $\chi^{(3)}_{1111}(\lambda=1.06\ \mu\text{m})/\chi^{(3)}_{1111}(\omega=0)$.

	ETB theory	Semi-*ab initio* theory	Experiment[a]	
Si	4	13	35	15
			56	23
			168	70
Ge	0.2	1.1	15	0.4
			25	0.6
			75	1.9
GaAs	0.8	6.6	22	5.6
			36	9.0
			108	27.0

[a]The left column is $\chi^{(3)}_{1111}$ (in units of 1×10^{-11} esu) measured using THG at $\lambda=1.06\ \mu$m from Ref. 19. These values of $\chi^{(3)}_{1111}$ were measured relative to LiF, and the relative values are Si, 7.2×10^4; Ge, 3.1×10^4; and GaAs, 4.5×10^4. (We have averaged their results for different surface preparations and geometries.) The top and middle rows for each material use the values for $\vec{\chi}^{(3)}$ of LiF from Ref. 25 made at $\lambda=0.69\ \mu$m using THG ($\vec{\chi}^{(3)}_{1111}=0.48\times10^{-14}$ esu) and four-wave-mixing experiments ($\vec{\chi}^{(3)}_{1111}=0.8\times10^{-14}$ esu). The bottom row uses the result for LiF from THG measurements at $\lambda=1.06\ \mu$m from Wang and Baardsen [Phys. Rev. **185**, 1079 (1969)], given as $\vec{\chi}^{(3)}_{1111}=2.4\times10^{-14}$ esu. Uncertainties for all measurements have been given as ~±50%. The right column is $\vec{\chi}^{(3)}_{1111}(\lambda=1.06\ \mu\text{m})/\vec{\chi}^{(3)}_{1111}(\lambda=10.6\ \mu\text{m})$ obtained using the results from this table and from Table VI.

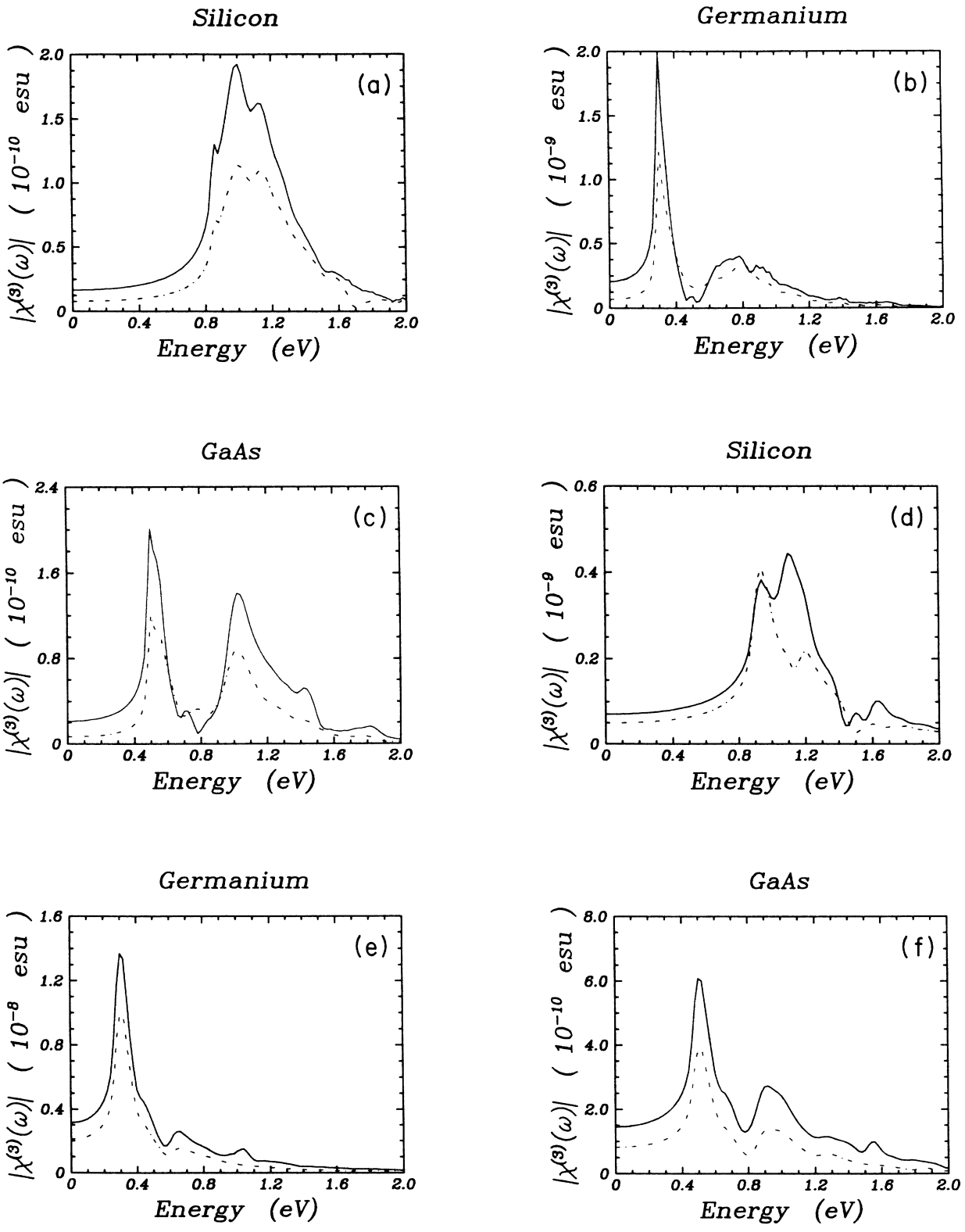

FIG. 4. Results for the dispersion in $|\vec{\chi}^{(3)}(\omega)|$ using the semi–*ab initio* tight-binding bands for (a) Si, (b) Ge, and (c) GaAs, and using the ETB bands for (d) Si, (e) Ge, and (f) GaAs. The dashed curves are $A \equiv |\chi^{(3)}_{1111}(\omega)|$ and the solid curves are $B \equiv 3|\chi^{(3)}_{1212}(\omega)|$.

tributions to $|\overleftrightarrow{\chi}^{(3)}(\omega)|$ from the 3ω resonance with the E_0 (at around 0.5 eV) and E_1 (at 1.0 eV) optical peaks that are comparable, primarily because the direct band gap and E_1 optical peak are closer together in energy than in Ge.

The only experimental data which exist for $|\overleftrightarrow{\chi}^{(3)}(\omega)|$ in these materials at wavelengths other than near $\lambda=10.6$ μm were measured using optical THG at $\lambda=1.06$ μm (Ref. 19) relative to $\overleftrightarrow{\chi}^{(3)}$ LiF at the same wavelength. Table VII shows the different values of $\overleftrightarrow{\chi}^{(3)}$ at $\lambda=1.06$ μm obtained by using various experimental results for $\overleftrightarrow{\chi}^{(3)}$ in LiF, together with the relative measurements of Ref. 19. Although a decrease in the ratio of $\overleftrightarrow{\chi}^{(3)}$ at $\lambda=1.06$ μm to that at $\lambda=10.6$ μm is seen both in the theory and experiment in going from Si and GaAs to Ge, a more conclusive assessment of the dispersion in $|\overleftrightarrow{\chi}^{(3)}(\omega)|$ is not possible because of the variation in the experimental results for $\overleftrightarrow{\chi}^{(3)}$ in LiF, and the uncertainty in the relative measurement of Ref. 19. In addition, at $\lambda=1.06$ μm in Si, the theoretical curve for $|\overleftrightarrow{\chi}^{(3)}(\omega)|$ decreases rapidly with energy, and so a small shift in the peak would have a large affect on this ratio.

C. Anisotropy

The theoretical and experimental results for the low-frequency limit of σ are shown in Table VIII. For all materials, the results obtained from the ETB bands agree quite well with experiment, while the results from the semi-*ab initio* tight-binding bands are significantly larger. The closest previous results in the literature are from Ref. 9, and were obtained by including local-field corrections. Their calculation showed that local-field corrections increased the anisotropy at low frequency, indicating that local-field corrections probably would not improve our results for the semi-*ab initio* tight-binding bands. The difference between the ETB and semi-*ab initio* tight-binding results again indicates the sensitivity of $\overleftrightarrow{\chi}^{(3)}$ to the band structure.

The dispersion of $|\sigma(\omega)|$ is shown in Fig. 5. The experimental results for silicon (from Ref. 11) represent the only measurements of dispersion in $\overleftrightarrow{\chi}^{(3)}$, and it is encouraging to see that the main spectral feature (the large peak near 1.4 eV) is indeed observed in both band-structure calculations, although shifted to slightly higher

TABLE VIII. Anisotropy results [shown is $|\sigma(\omega=0)|\equiv|3\chi^{(3)}_{1212}(0)/\chi^{(3)}_{1111}(0)-1|$].

	Si	Ge	GaAs
Theory (ETB)	0.43	0.49	0.77
Theory (semi-*ab initio*)	1.09	2.02	2.10
VA[a]	0.98	1.02	0.95
Experiment	0.44±0.1[b]	0.56±0.03[c]	0.59±0.15[c]
		0.83±0.06[b]	

[a]From Ref. 9. Their results are related to ours by $\overleftrightarrow{\chi}^{(3)}_{\langle 1111\rangle}/\overleftrightarrow{\chi}^{(3)}_{\langle 100\rangle}=\frac{2}{3}\sigma+1$.
[b]From Ref. 17.
[c]From Ref. 26.

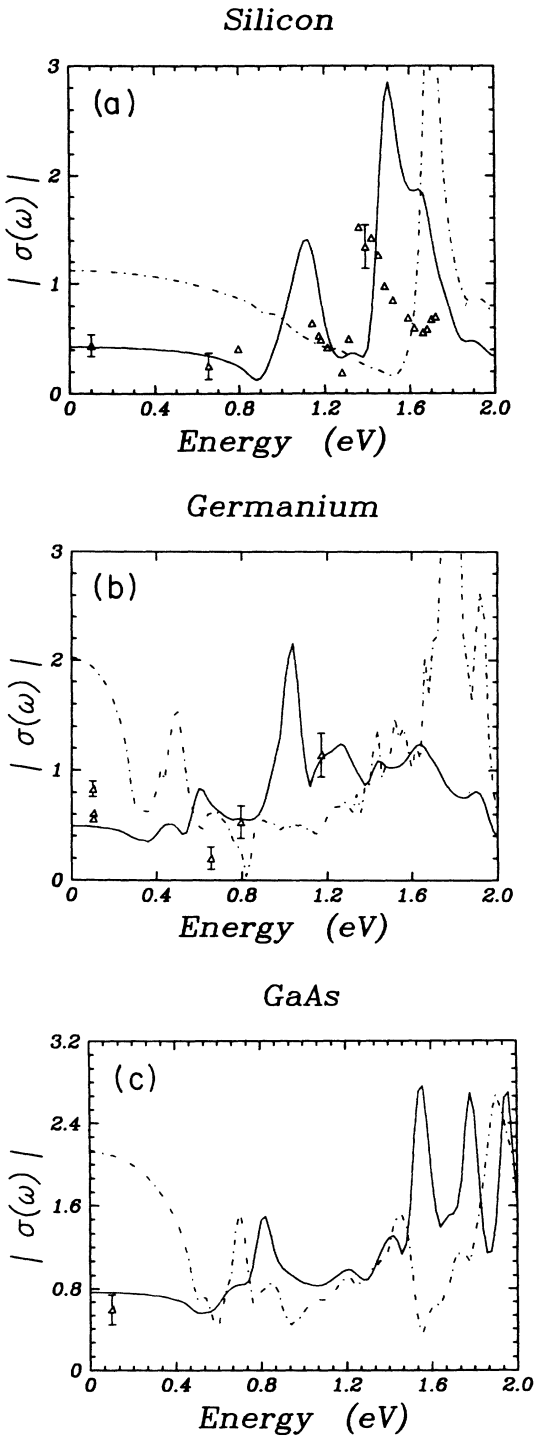

FIG. 5. Dispersion in the magnitude of the anisotropy [$|\sigma(\omega)|$ defined in the text] for (a) Si, (b) Ge, and (c) GaAs. The solid lines represent the theoretical results using ETB bands, the dashed lines are the results from the semi-*ab initio* tight-binding bands, and the points are experimental data. The experimental results at $\lambda=10.6$ μm are listed in Table VIII, and we also show the results for Ge of C. C. Wang and N. W. Ressler [Phys. Rev. B 2, 1827 (1970)]. The results at other frequencies for Si are from Ref. 11 and for Ge from Ref. 12. The ETB results for Si are slightly different than those shown in Ref. 11, which were preliminary calculations.

energies. In addition, the small peak near 1.0 eV present in the experimental data is also present in the ETB calculation. The peak around 1.5 eV arises from the dip between the two peaks in $|\overleftrightarrow{\chi}^{(3)}_{1111}(\omega)|$ discussed in the preceding section, while the small bump is due to the 3ω resonance with the E_1 critical point. We see, therefore, that $|\sigma(\omega)|$ and $|\overleftrightarrow{\chi}^{(3)}(\omega)|$ are sensitive to different features in the band structure. For Ge the dominant feature in the theoretical curve for $|\sigma(\omega)|$ from the ETB bands is a peak near 1.0 eV, from the ω resonance with the direct band gap. Although the experimental data seem to be consistent with this, three data points are not sufficient to assess the agreement between theory and experiment. Finally, we mention that no experimental data exist for σ in GaAs (to our knowledge) at wavelengths other than $\lambda=10.6$ μm. Nonetheless, we show the dispersion in $|\sigma(\omega)|$ for GaAs in Fig. 5(c), where we see that, again, features in $|\sigma|$ occur at energies other than where they occur for $|\overleftrightarrow{\chi}^{(3)}(\omega)|$. (Note that in measuring σ in noncentrosymmetric materials, one must account for the two-step contribution to THG, as has been done for GaAs.[26] We expect the theoretical results from the ETB calculation for the dispersion in σ for GaAs to be as good as or better than for Ge since the ETB bands were more successful for GaAs in calculating both the linear-optical properties and $\overleftrightarrow{\chi}^{(3)}(0)$. Finally, we show the relative phase of B/A ($\equiv\phi$) for Si and Ge in Fig. 6, along with the experimental results from Refs. 11 and 12. Again, agreement between theory and experiment is good. The relative phase of B/A also shows structure where the magnitude of the anisotropy does.

It is evident, then, that structure in the anisotropy tends to occur at different energies from where structure in the magnitude of $\overleftrightarrow{\chi}^{(3)}$ occurs. This arises primarily because $\sigma(\omega)$ is not dominated by 3ω resonances, in contrast with $|\overleftrightarrow{\chi}^{(3)}(\omega)|$, since it does not contain the strong frequency dependence that enhances features lower in energy for $|\overleftrightarrow{\chi}^{(3)}(\omega)|$.

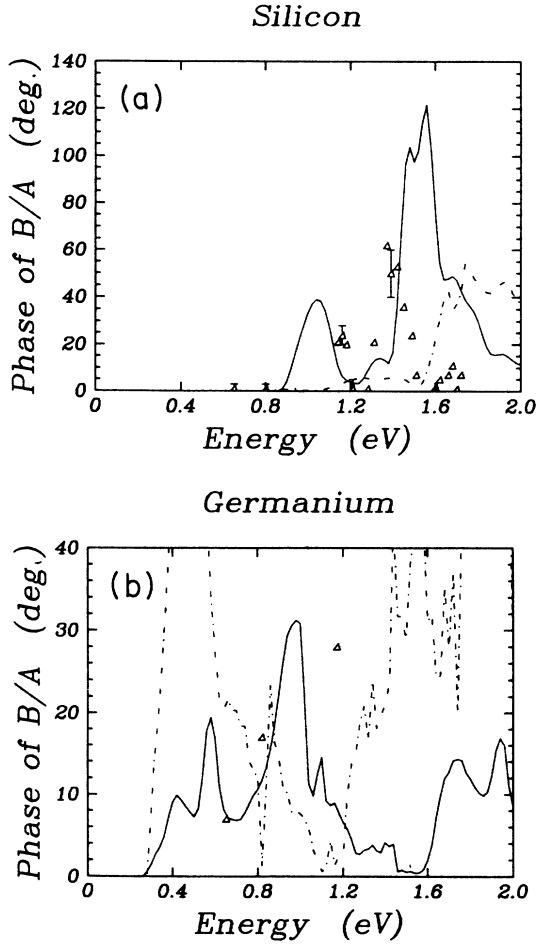

FIG. 6. Dispersion in the relative phase of B/A ($B/A=|B/A|e^{i\phi}$) for (a) Si and (b) Ge. The experimental data points are from Ref. 11 for silicon and Ref. 12 for germanium. The solid curves are the theoretical results from the ETB calculation, while the dashed curves are from the semi-*ab initio* tight-binding bands. The magnitude of ϕ is shown, since there is an experimental ambiguity in sign.

VI. CONCLUSIONS

We have performed full band-structure calculations of the magnitude, dispersion, and anisotropy in the nonlinear response $\overleftrightarrow{\chi}^{(3)}$ for optical third-harmonic generation in Si, Ge, and GaAs. We accomplished this using both an empirical tight-binding and semi-*ab initio* tight-binding band-structure technique. The calculation was performed with the minimal-coupling (MC), or "$\mathbf{p}\cdot\mathbf{A}$," interaction Hamiltonian, using standard perturbation theory within the RPA and neglecting local-field corrections.

The results for $\overleftrightarrow{\chi}^{(3)}(0)$ from the ETB bands typically overestimated the experimental results (although for Si and GaAs were approximately within the experimental error), while the semi-*ab initio* results tended to underestimate the experimental results. Our results for $\overleftrightarrow{\chi}^{(3)}(0)$ were better than the only other full band-structure calculation to date,[4] but not quite as good as a limited band-structure calculation[8] of $\overleftrightarrow{\chi}^{(3)}(0)$ which modeled the energy bands around the main critical points responsible for the linear-optical absorption spectrum. This indicates that $\overleftrightarrow{\chi}^{(3)}(0)$ is very sensitive to the joint density of states at the critical points in the energy bands.

We found that the sign of $\overleftrightarrow{\chi}^{(3)}(0)$ obtained using the MC Hamiltonian is, in general, positive for all elements and that $\overleftrightarrow{\chi}^{(3)}(0)$ was dominated by the interband response. Results for $\overleftrightarrow{\chi}^{(3)}(0)$ obtained using the dipole Hamiltonian[8,9] indicating that the positive sign is due to the contribution of intraband terms reflect the fact that the relative contribution of intraband and interband terms are different when $\overleftrightarrow{\chi}^{(3)}$ is calculated using the MC and dipole interaction Hamiltonians, even though both expressions are equivalent. This phenomenon has previously been noted[15] in connection with $\overleftrightarrow{\chi}^{(2)}$ in zinc-blende materials.

Although the magnitude of $\overleftrightarrow{\chi}^{(3)}$ calculated with the

ETB and semi-*ab initio* band structures differed significantly, the structure in the dispersion of $\overleftrightarrow{\chi}^{(3)}(\omega)$ was remarkably similar. Because of the strong energy dependence of $\overleftrightarrow{\chi}^{(3)}$ the spectrum of $|\overleftrightarrow{\chi}^{(3)}(\omega)|$ was dominated by 3ω resonances with features in the energy bands near the band gap. Unfortunately, the paucity of experimental results made comparison with theory for the dispersion in $|\overleftrightarrow{\chi}^{(3)}(\omega)|$ inconclusive.

Our results for the zero-frequency limit of the anisotropy in $\overleftrightarrow{\chi}^{(3)}$ from the ETB calculations agreed well with experiment for all materials, while the corresponding results from the semi-*ab initio* bands were overestimated by roughly a factor of 2–3. This indicates the high degree of sensitivity of $\overleftrightarrow{\chi}^{(3)}$ to the electronic band structure. For Si there was also good agreement with recent measurements of the dispersion in the anisotropy at frequencies comparable to the band gap. Finally, our general agreement between theory and experiment for the anisotropy suggests that the failure of earlier models to successfully predict this quantity in Si, Ge, and GaAs was due predominantly to the neglect of, or inadequate approach to, the band-structure nature of solids. The large sensitivity of $\overleftrightarrow{\chi}^{(3)}$ to details of the electronic band-structure, however, prevents us from concluding categorically that local-field corrections are negligible in determining the nonlinear-optical properties of bulk semiconductors.

ACKNOWLEDGMENTS

We gratefully acknowledge Professor W. Y. Ching for providing us with his data. We also acknowledge financial support from the Natural Sciences and Engineering Research Council (NSERC) of Canada.

APPENDIX

Although expressions for the nonlinear response functions in solids have been presented before,[4,5] the connection between states of the system and single-particle states has not always been clear. For this reason, we present in some detail the derivation of the nonlinear-optical response in solids, including effects up to third order in the incident fields.

For a closed system subjected to an external perturbation $V(t)$, we have

$$\dot{\rho}=\frac{1}{i\hbar}[\mathcal{H},\rho]\ ,\qquad \mathcal{H}=\mathcal{H}_0+V(t)\ , \tag{A1}$$

where ρ is the density-matrix operator for the system, and $\mathcal{H}$ and $\mathcal{H}_0$ are the total and unperturbed Hamiltonians, respectively. Writing

$$\rho=\mathcal{S}^{\dagger}(t)\sigma(t)\mathcal{S}(t)\ ,\qquad \mathcal{S}(t)=e^{i\mathcal{H}_0 t/\hbar}\ , \tag{A2}$$

then Eq. (A1) becomes

$$\dot{\sigma}=\frac{1}{i\hbar}[\bar{V}(t),\sigma(t)]\ ,\qquad \bar{V}(t)=\mathcal{S}(t)V(t)\mathcal{S}^{\dagger}(t)\ . \tag{A3}$$

As the zeroth-order solution [in $\bar{V}(t)$] we take $\sigma(t)=\sigma_0$ and then iterate to obtain

$$\sigma(t)=\sigma_0+\frac{1}{i\hbar}\int_{-\infty}^{t}[\bar{V}(t'),\sigma_0]dt'+\left[\frac{1}{i\hbar}\right]^2\int_{-\infty}^{t}\int_{-\infty}^{t'}[\bar{V}(t'),[\bar{V}(t''),\sigma_0]]dt''\,dt'$$
$$+\left[\frac{1}{i\hbar}\right]^3\int_{-\infty}^{t}\int_{-\infty}^{t'}\int_{-\infty}^{t''}[\bar{V}(t'),[\bar{V}(t''),[\bar{V}(t'''),\sigma_0]]]dt'''\,dt''\,dt'+\cdots\ . \tag{A4}$$

The expectation value of an operator $\mathcal{O}(t)$ is given by

$$\langle\mathcal{O}(t)\rangle=\mathrm{Tr}[\rho(t)\mathcal{O}(t)]=\mathrm{Tr}[\sigma(t)\bar{\mathcal{O}}(t)]\ . \tag{A5}$$

Using the trace identity for three operators (A,B,C),

$$\mathrm{Tr}([A,B]C)=\mathrm{Tr}(B[C,A])\ , \tag{A6}$$

Eq. (A4) can be "unraveled" to give

$$\langle\mathcal{O}(t)\rangle=\mathrm{Tr}[\sigma_0\mathcal{O}(t)]\ , \tag{A7}$$

where,

$$\mathcal{O}(t)=\frac{1}{i\hbar}\int_{-\infty}^{t}[\bar{\mathcal{O}}(t),\bar{V}(t')]dt'+\left[\frac{1}{i\hbar}\right]^2\int_{-\infty}^{t}\int_{-\infty}^{t'}[[\bar{\mathcal{O}}(t),\bar{V}(t')],\bar{V}(t'')]dt''\,dt'$$
$$+\left[\frac{1}{i\hbar}\right]^3\int_{-\infty}^{t}\int_{-\infty}^{t'}\int_{-\infty}^{t''}[[[\bar{\mathcal{O}}(t),\bar{V}(t')],\bar{V}(t'')],\bar{V}(t''')]dt'''\,dt''\,dt'+\cdots\ . \tag{A8}$$

The operators $\mathcal{O}(t)$, $\bar{V}(t)$ are for the entire system; in order to proceed we choose to expand these operators in terms of single-particle operators. In our calculation we treat the electromagnetic fields classically, and so in a solid we can write the perturbation in terms of single-particle operators as

$$V(t)=\sum_{i,j} V_{ij}(t)a_i^\dagger a_j \ , \tag{A9}$$

where $a^\dagger, a$ are fermion creation and annihilation operators, respectively, for electrons in a solid, and i,j run over all single-particle states. If we further assume that the particles are independent, we have

$$\mathcal{H}_0=\sum_s \hbar\omega_s a_s^\dagger a_s \ , \tag{A10}$$

and so

$$\bar{V}(t)=\sum_{i,j} a_i^\dagger a_j \bar{V}_{ij}(t) \ , \tag{A11}$$

with

$$\bar{V}_{ij}(t)=e^{i\omega_{ij}t}V_{ij}(t) \ , \tag{A12}$$

where $\omega_{ij}=\omega_i-\omega_j$, and there is a similar equation for $\mathcal{O}(t)$. Next, we substitute Eqs. (A9)–(A12) into (A8), and make use of the following relations:

$$\begin{aligned}
&\{a_i,a_j^\dagger\}\equiv a_i a_j^\dagger + a_j^\dagger a_i=\delta_{ij} \ , \\
&[a_i^\dagger a_j,\, a_k^\dagger a_l]=a_i^\dagger a_j a_k^\dagger a_l - a_k^\dagger a_l a_i^\dagger a_j = a_i^\dagger a_l \delta_{kj} - a_k^\dagger a_j \delta_{il} \ , \\
&[[a_i^\dagger a_j,\, a_k^\dagger a_l],\, a_m^\dagger a_n]=(a_i^\dagger a_n \delta_{lm} - a_m^\dagger a_l \delta_{in})\delta_{kj} - (a_k^\dagger a_n \delta_{jm} - a_m^\dagger a_j \delta_{kn})\delta_{il} \ ,
\end{aligned} \tag{A13}$$

and so on. From these it follows that

$$\begin{aligned}
&\mathrm{Tr}(\sigma_0 a_i^\dagger a_j)=\delta_{ij} f_i \ , \\
&\mathrm{Tr}(\sigma_0[a_i^\dagger a_j,\, a_k^\dagger a_l])=f_{ij}\delta_{il}\delta_{kj} \ , \\
&\mathrm{Tr}(\sigma_0[[a_i^\dagger a_j,\, a_k^\dagger a_l],\, a_m^\dagger a_n])=f_{il}\delta_{in}\delta_{jk}\delta_{lm}+f_{jk}\delta_{il}\delta_{jm}\delta_{kn} \ , \\
&\mathrm{Tr}(\sigma_0[[[a_i^\dagger a_j,\, a_k^\dagger a_l],\, a_m^\dagger a_n],\, a_o^\dagger a_p])=f_{in}\delta_{ip}\delta_{jk}\delta_{lm}\delta_{no}+f_{ln}\delta_{in}\delta_{jk}\delta_{lo}\delta_{mp}+f_{nk}\delta_{il}\delta_{jm}\delta_{kp}\delta_{no}+f_{mj}\delta_{il}\delta_{jo}\delta_{kn}\delta_{mp} \ ,
\end{aligned} \tag{A14}$$

where f_i is the Fermi factor for state i, and $f_{ij}=f_i-f_j$. Therefore, making use of Eqs. (A13) and (A14), we obtain

$$\begin{aligned}
\langle \mathcal{O}(t)\rangle &= \mathrm{Tr}[\sigma_0 \mathcal{O}(t)] \\
&= \langle \mathcal{O}(t)\rangle^{(0)} + \langle \mathcal{O}(t)\rangle^{(1)} + \langle \mathcal{O}(t)\rangle^{(2)} + \langle \mathcal{O}(t)\rangle^{(3)} + \cdots \ ,
\end{aligned} \tag{A15}$$

where

$$\begin{aligned}
&\langle \mathcal{O}(t)\rangle^{(0)} = f_i \bar{\mathcal{O}}_{ii}(t) \ , \\
&\langle \mathcal{O}(t)\rangle^{(1)} = \frac{f_{ij}}{i\hbar}\bar{\mathcal{O}}_{ij}(t)\int_{-\infty}^{t}\bar{V}_{ji}(t')dt' \ , \\
&\langle \mathcal{O}(t)\rangle^{(2)} = \frac{f_{ik}}{(i\hbar)^2}\bar{\mathcal{O}}_{ij}(t)\int_{-\infty}^{t}\int_{-\infty}^{t'}\bar{V}_{jk}(t')\bar{V}_{kl}(t'')dt''\,dt' + \frac{f_{jk}}{(i\hbar)^2}\bar{\mathcal{O}}_{ij}(t)\int_{-\infty}^{t}\int_{-\infty}^{t'}\bar{V}_{ki}(t')\bar{V}_{jk}(t'')dt''\,dt' \ , \\
&\langle \mathcal{O}(t)\rangle^{(3)} = \frac{f_{il}}{(i\hbar)^3}\bar{\mathcal{O}}_{ij}(t)\int_{-\infty}^{t}\int_{-\infty}^{t'}\int_{-\infty}^{t''}V_{jk}(t')\bar{V}_{kl}(t'')\bar{V}_{li}(t''')dt'''\,dt''\,dt' \\
&\qquad + \frac{f_{kl}}{(i\hbar)^3}\bar{\mathcal{O}}_{ij}(t)\int_{-\infty}^{t}\int_{-\infty}^{t'}\int_{-\infty}^{t''}\bar{V}_{jk}(t')\bar{V}_{li}(t'')\bar{V}_{kl}(t''')dt'''\,dt''dt' \\
&\qquad + \frac{f_{kl}}{(i\hbar)^3}\mathcal{O}_{ij}(t)\int_{-\infty}^{t}\int_{-\infty}^{t'}\int_{-\infty}^{t''}\bar{V}_{li}(t')\bar{V}_{jk}(t'')\bar{V}_{kl}(t''')dt'''\,dt''\,dt' \\
&\qquad + \frac{f_{kj}}{(i\hbar)^3}\bar{\mathcal{O}}_{ij}(t)\int_{-\infty}^{t}\int_{-\infty}^{t'}\int_{-\infty}^{t''}\bar{V}_{li}(t')\bar{V}_{kl}(t'')\bar{V}_{jk}(t''')dt'''\,dt''\,dt' \ ,
\end{aligned} \tag{A16}$$

and where repeated indices are summed over. Now, if we assume the perturbation contains discrete frequencies, then we can write

$$\bar{V}_{ij}(t)=\sum_\alpha \bar{V}_{ij}^{(\alpha)}e^{-i\omega_\alpha t} \ , \tag{A17}$$

and so [with the aid of (A3)] we obtain

$$\langle \mathcal{O}(t)\rangle^{(1)}=G_{ij}^{(1)}(\alpha)\mathcal{O}_{ij}V_{ji}^{(\alpha)}e^{-i\omega_\alpha t},$$
$$\langle \mathcal{O}(t)\rangle^{(2)}=G_{ijk}^{(2)}(\alpha\beta)\mathcal{O}_{ij}V_{jk}^{(\alpha)}V_{ki}^{(\beta)}e^{-i(\omega_\alpha+\omega_\beta)t}, \tag{A18}$$
$$\langle \mathcal{O}(t)\rangle^{(3)}=G_{ijkl}^{(3)}(\alpha\beta\gamma)\mathcal{O}_{ij}V_{jk}^{(\alpha)}V_{kl}^{(\beta)}V_{li}^{(\gamma)}e^{-i(\omega_\alpha+\omega_\beta+\omega_\gamma)t},$$

where all repeated indices, including α, β, and γ, are summed over, and where

$$G_{ij}^{(1)}(\alpha)=\frac{f_{ij}}{E_\alpha-E_{ji}},$$
$$G_{ijk}^{(2)}(\alpha,\beta)=\frac{1}{E_\alpha+E_\beta-E_{ji}}\left[\frac{f_{ik}}{E_\beta-E_{ki}}+\frac{f_{jk}}{E_\alpha-E_{jk}}\right], \tag{A19}$$
$$G_{ijkl}^{(3)}(\alpha,\beta,\gamma)=\frac{1}{E_\alpha+E_\beta+E_\gamma-E_{ji}}\left[\frac{1}{E_\beta+E_\gamma-E_{ki}}\left[\frac{f_{il}}{E_\gamma-E_{li}}+\frac{f_{kl}}{E_\beta-E_{kl}}\right]+\frac{1}{E_\alpha+E_\beta-E_{jl}}\left[\frac{f_{kj}}{E_\alpha-E_{jk}}+\frac{f_{kl}}{E_\beta-E_{kl}}\right]\right],$$

with no summation implied. Here, $E_\alpha=\hbar\omega_\alpha$, etc., and $E_{ji}=E_j-E_i$. This gives the nonlinear response of the solid at all frequencies as α,β,γ are summed over. In practice, one is usually interested in that response at only a particular frequency, and one simply sums over all permutations of the frequencies α,β,γ. Note that the sums over i,j,k,l in Eqs. (A18) run over *all* single-particle states.

If we explicitly consider the *optical* nonlinear response of a solid, then the total Hamiltonian of the system is

$$\mathcal{H}=\mathcal{H}_0+\mathcal{H}^{\mathrm{I}}+\mathcal{H}^{\mathrm{II}}, \tag{A20}$$

where

$$\mathcal{H}_0=\frac{1}{2m}\sum_i|\mathbf{p}_i|^2+\sum_i U(\mathbf{r}_i),$$
$$\mathcal{H}^{\mathrm{I}}=-\frac{e}{2mc}\sum_i[\mathbf{p}_i\cdot\mathbf{A}(\mathbf{r}_i,t)+\mathbf{A}(\mathbf{r}_i,t)\cdot\mathbf{p}_i]+\sum_i e\phi(\mathbf{r}_i,t), \tag{A21}$$
$$\mathcal{H}^{\mathrm{II}}=\frac{e^2}{2mc^2}\sum_i\mathbf{A}(\mathbf{r}_i,t)\cdot\mathbf{A}(\mathbf{r}_i,t),$$

and where $U(\mathbf{r}_i)$ is the static crystal potential. In the usual fashion, we make the perturbation calculation as if ϕ and $\mathbf{A}$ were incident fields, and then replace them by the sum of the incident field and the classical field that would be generated by the expectation value of the charge-current density. We further neglect local-field corrections by then replacing those sums by the potentials which describe the macroscopic electromagnetic fields. Adopting the radiation gauge ($\phi=0$) and making the dipole approximation [$\mathbf{A}(\mathbf{r}_i,t)\rightarrow\mathbf{A}(t)$], and using Eq. (A9), we obtain

$$\mathcal{H}^{\mathrm{I}}\simeq\frac{e}{mc}a_k^\dagger a_l\mathbf{p}_{kl}\cdot\mathbf{A}(t),$$
$$\mathcal{H}^{\mathrm{II}}\simeq\frac{e^2}{2mc^2}a_k^\dagger a_l\delta_{kl}\mathbf{A}(t)\cdot\mathbf{A}(t), \tag{A22}$$

and

$$\mathbf{A}(t)=\mathbf{A}^{(\alpha)}e^{-i\omega_\alpha t},$$
$$\mathbf{E}(t)=-\frac{1}{c}\dot{\mathbf{A}}(t)=\frac{i\omega_\alpha}{c}\mathbf{A}^{(\alpha)}e^{-i\omega_\alpha t} \tag{A23}$$
$$=\mathbf{E}^{(\alpha)}e^{-i\omega_\alpha t},$$

again summing over all repeated Greek and Roman indices.

Finally, we are interested in finding the nonlinear polarization current density in the medium, and so we take (in the dipole approximation)

$$\mathcal{O}(t)=\sum_i\mathbf{j}_i(t)$$
$$=\sum_i\frac{e}{m}\left[\mathbf{p}_i-\frac{e}{c}\mathbf{A}(t)\right]$$
$$=\dot{\boldsymbol{\mu}}(t)$$
$$\equiv\mathcal{O}^{(0)}+\mathcal{O}^{(1)}. \tag{A24}$$

Using Eqs. (A18), we solve for the macroscopic nonlinear polarization $\mathbf{P}=\boldsymbol{\mu}/V$, where V is the normalization volume of the system. It follows that $\mathcal{H}^{\mathrm{II}}$ yields no contribution (to any order) to $\langle\mathbf{P}\rangle$, and that $\mathcal{O}^{(1)}$ only contributes to $\langle\mathbf{P}\rangle^{(1)}$. Finally, we write the macroscopic dipole-moment density as

$$P_a^{(1)}(t)=\sum_{b,\alpha}\chi_{ab}^{(1)}(-\omega_\alpha;\omega_\alpha)\mathcal{E}_b^\alpha e^{-i\omega_\alpha t},$$
$$P_a^{(2)}(t)=\sum_{b,c,\alpha,\beta}\chi_{abc}^{(2)}(-\omega_\alpha-\omega_\beta;\omega_\alpha,\omega_\beta)\mathcal{E}_b^\alpha\mathcal{E}_c^\beta e^{-i(\omega_\alpha+\omega_\beta)t}, \tag{A25}$$
$$P_a^{(3)}(t)=\sum_{b,c,d,\alpha,\beta,\gamma}\chi_{abcd}^{(3)}(-\omega_\alpha-\omega_\beta-\omega_\gamma;\omega_\alpha,\omega_\beta,\omega_\gamma)\mathcal{E}_b^\alpha\mathcal{E}_c^\beta\mathcal{E}_d^\gamma e^{-i(\omega_\alpha+\omega_\beta+\omega_\gamma)t},$$

where

$$\chi^{(1)}_{ab}(-\omega_\alpha;\omega_\alpha)=-\sum_{i,j}\left[\frac{e}{m\omega_\alpha}\right]^2 G^{(1)}_{ij}(\alpha)p^a_{ij}p^b_{ji}-\frac{e^2n_0}{m\omega_\alpha}\delta^{ab}\ ,$$

$$\chi^{(2)}_{abc}(-\omega_\alpha-\omega_\beta;\omega_\alpha,\omega_\beta)=-\sum_{i,j,k}\frac{ie^3}{m^3\omega_\alpha\omega_\beta(\omega_\alpha+\omega_\beta)}G^{(2)}_{ijk}(\alpha,\beta)p^a_{ij}p^b_{jk}p^c_{ki}\ , \tag{A26}$$

$$\chi^{(3)}_{abcd}(-\omega_\alpha-\omega_\beta-\omega_\gamma;\omega_\alpha,\omega_\beta,\omega_\gamma)=\sum_{i,j,k,l}\frac{e^4}{m^4\omega_\alpha\omega_\beta\omega_\gamma(\omega_\alpha+\omega_\beta+\omega_\gamma)}G^{(3)}_{ijkl}(\alpha,\beta,\gamma)p^a_{ij}p^b_{jk}p^c_{kl}p^d_{li}\ ,$$

with $G^{(1)}$, $G^{(2)}$, etc., as defined in Eqs. (A19); only the indices explicitly indicated to be summed over. Here, n_0 is the number of electrons per unit volume, and the f_i appearing in the G's are now to be interpreted as Fermi factors per unit volume. Note that χ's are not symmetric with respect to α,β,γ, but if all frequencies are summed over in Eqs. (A25), this does not matter.

---

*Present address: Division of Physics, National Research Council of Canada, Ottowa, Ontario, Canada K1A OR6.

[1]D. J. Moss, J. E. Sipe, and H. M. van Driel, Phys. Rev. B **36**, 9708 (1987).

[2]C. Y. Fong and Y. R. Shen, Phys. Rev. B **12**, 2325 (1975).

[3]S. Janz, H. M. van Driel, and J. E. Sipe (unpublished).

[4]K. Arya and S. S. Jha, Phys. Rev. B **20**, 1611 (1979).

[5]S. S. Jha and N. Bloembergen, Phys. Rev. **171**, 891 (1968).

[6]J. C. Phillips and J. A. Van Vechten, Phys. Rev. **183**, 709 (1969).

[7]C. Flytzanis, Phys. Lett. **31A**, 273 (1970).

[8]J. A. van Vechten and D. E. Aspnes, Phys. Lett. **30A**, 346 (1969).

[9]J. A. van Vechten, M. Cardona, D. E. Aspnes, and R. M. Martin, in *Proceedings of the Tenth International Conference on the Physics of Semiconductors,* Cambridge, Mass., 1970, edited by S. P. Keller, J. C. Hensel and F. Stern (U.S. AEC Division of Technical Information Extension, Oak Ridge, Tenn. 1970), p. 82.

[10]J. E. Sipe, D. J. Moss, and H. M. van Driel, Phys. Rev. B **35**, 1129 (1987).

[11]D. J. Moss, H. M. van Driel, and J. E. Sipe, Opt. Lett. **14**, 57 (1989).

[12]D. J. Moss, Ph.D. thesis, University of Toronto, 1988 (unpublished).

[13]D. J. Moss, E. Ghahramani, J. E. Sipe, and H. M. van Driel, Phys. Rev. B **34**, 8758 (1986).

[14]M. Z. Huang and W. Y. Ching, J. Phys. Chem. Solids **46**, 977 (1985).

[15]D. E. Aspnes, Phys. Rev. B **6**, 4648 (1972).

[16]D. E. Aspnes, Phys. Rev. **153**, 972 (1972); D. E. Aspnes, P. Handler, and D. F. Blossy, *ibid.* **166**, 921 (1968).

[17]J. J. Wynne and G. D. Boyd, Appl. Phys. Lett. **12**, 191 (1968); J. J. Wynne, Phys. Rev. **178**, 1295 (1969).

[18]M. I. Bell, in *Electronic Density of States,* Nat. Bur. Stand. (U.S.) Spec. Publ. No. 323, edited by L. H. Bennet (U.S. GPO, Washington, D.C., 1971), p. 757.

[19]W. K. Burns and N. Bloembergen, Phys. Rev. B **4**, 3437 (1971).

[20]J. R. Chelikowsky and M. L. Cohen, Phys. Rev. B **14**, 556 (1976).

[21]C. Flytzanis, *Quantum Electronics,* edited by H. Rabin and C. L. Tang (Academic, New York, 1975), p. 9.

[22]M. Cardona, J. Phys. Chem. Solids **24**, 1543 (1963).

[23]D. J. Moss, J. E. Sipe, and H. M. van Driel, Phys. Rev. B **36**, 1153 (1987).

[24]We point out that the results of Ref. 4 are actually not as good as they appear in that paper. There are two definitions for $\vec{\chi}^{(3)}$—that of Maker and Terhune (MT) (Ref. 9) ($c^{(3)}_{1111}$) and that which is a factor of 4 larger.[5] Equation (37) in Ref. 4 for $\vec{\chi}^{(3)}(0)$ uses the latter definition, while the experimental results quoted in Ref. 4 use MT's definition. From Table VI, therefore, we see that their result for Si is approximately an order of magnitude too small, while their result for Ge is almost 2 orders of magnitude too small. As the authors pointed out, their band structure was crude since it only included first-nearest-neighbor interactions, and, as we have seen, $\vec{\chi}^{(3)}(0)$ is quite sensitive to details of the band structure. In addition, they incorrectly treat the (singular) dipole interaction matrix elements in a solid. Nonetheless, the work in Ref. 4 represents a significant improvement over molecular-orbital methods towards understanding $\vec{\chi}^{(3)}$ in solids.

[25]P. D. Maker and R. W. Terhune, Phys. Rev. **137**, A801 (1965).

[26]E. Yablonovitch, C. Flytzanis, and N. Bloembergen, Phys. Rev. Lett. **29**, 865 (1972).